Title

Nucleoside/nucleotide reverse transcriptase inhibitors attenuate angiogenesis and lymphangiogenesis by impairing receptor tyrosine kinases signalling in endothelial cells

Authors

Song, Lin
Ding, Sha
Ge, Zhen
et al.

Peer reviewed

RESEARCH PAPER

Nucleoside/nucleotide reverse transcriptase inhibitors attenuate angiogenesis and lymphangiogenesis by impairing receptor tyrosine kinases signalling in endothelial cells

Correspondence Luyang Yu, Institute of Genetics and Regenerative Biology, College of Life Sciences, Zhejiang University, No. 866 Yuhangtang Road, Hangzhou, Zhejiang 310058, China. E-mail: luyangyu@zju.edu.cn

Lin Song[1,2,5,*], Sha Ding[1,2,5,*], Zhen Ge[3], Xiaolong Zhu[1,2,5], Cong Qiu[1,2,5], Yuewen Wang[1,2,5], Enyin Lai[4], Weijun Yang[1], Yi Sun[1], Samson A Chow[6] and Luyang Yu[1,2,5] ![ORCID]

[1]*Institute of Genetics and Regenerative Biology, College of Life Sciences, Zhejiang University, Hangzhou, Zhejiang, China,* [2]*Research Center for Air Pollution and Health, Zhejiang University, Hangzhou, Zhejiang, China,* [3]*Institute of Materia Medica, Zhejiang Academy of Medical Sciences, Hangzhou, Zhejiang, China,* [4]*Department of Physiology, School of Medicine, Zhejiang University, Hangzhou, Zhejiang, China,* [5]*Key Laboratory for Cell and Gene Engineering of Zhejiang Province, Hangzhou, Zhejiang, China, and* [6]*Department of Molecular and Medical Pharmacology, University of California, Los Angeles, CA, USA*

*These authors contributed equally to this work.

BACKGROUND AND PURPOSE

Cardiovascular disease associated with antiretroviral therapy (ART) has become a major clinical challenge for HIV-positive patients. However, the role of ART in blood vessel growth is largely unknown. Here, we examined an integral component of ART, nucleoside/nucleotide reverse transcriptase inhibitors (NRTIs) and investigated their effects on key microvascular functions, including angiogenesis and lymphangiogenesis.

EXPERIMENTAL APPROACH

The angiogenesis/lymphangiogenesis capability of endothelial cells (ECs) was evaluated using migration, proliferation and tube formation assays *in vitro*, and mouse ear and Matrigel plug assays *in vivo*. Expressions of signalling molecules and mitochondrial antioxidant catalases were determined using Western blotting. Receptor tyrosine kinase (RTK) internalization and endocytosis were examined using flow cytometry and confocal immunofluorescence microscopy respectively. Mitochondrial DNA copy number and ROS were determined using quantitative real-time PCR and MitoSOX staining respectively.

KEY RESULTS

Pharmaceutical doses of NRTIs [azidothymidine (AZT), tenofovir disoproxil fumarate (TDF) and lamivudine (3TC)] inhibited angiogenesis and lymphangiogenesis both *in vivo* and *in vitro* by affecting the proliferation and migration of ECs. Correspondingly, NRTIs selectively attenuated the activation and transduction of endothelial RTK signals, VEGFR2 and FGFR1 pathways, in vascular ECs and the VEGFR3 pathway in lymphatic ECs. Both TDF and 3TC restrained RTKs' endocytosis into early endosomes but not internalization, while AZT blocked the protein maturation of RTKs. Excessive ROS levels were detected in NRTI-treated ECs, and the MnSOD mimic MnTMPyP alleviated the angiogenic/lymphangiogenic defects induced by NRTIs.

CONCLUSIONS AND IMPLICATIONS

NRTIs negatively regulate angiogenesis and lymphangiogenesis by inducing mitochondrial oxidative stress and subsequently impairing RTK signalling in ECs.

Abbreviations

3TC, lamivudine; ART, antiretroviral therapy; AZT, azidothymidine; CVD, cardiovascular disease; MnSOD, recombinant human superoxide dismutase; MnTMPyP, manganese (III) tetrakis (N-methyl-2-pyridyl) porphyrin; NRTIs, nucleoside/nucleotide reverse transcriptase inhibitors; OCT, optimal cutting temperature compound; PI, protease inhibitors; RTK, receptor tyrosine kinase; TDF, tenofovir disoproxil fumarate; TRX2, thioredoxin protein 2

Introduction

The development of nucleoside/nucleotide reverse transcriptase inhibitors (NRTIs) in 1987 has provided a highly successful antiretroviral therapy (ART) and made HIV infection a manageable clinical entity (Massimo Andreoni *et al.,* 2015; Bhatti *et al.,* 2016; Ray *et al.,* 2016). The clinical challenges now confronting HIV-positive patients have shifted significantly from AIDS to chronic non-communicable diseases, among which cardiovascular disease (CVD) is a major issue (Triant *et al.,* 2007; Lang *et al.,* 2010; Baker and Lundgren, 2011; Boccara *et al.,* 2013; Freiberg *et al.,* 2013; Hemkens and Bucher, 2014; Althoff *et al.,* 2015). Recently, the National Heart, Lung, and Blood Institute (NHLBI) of the NIH recognized the high rates of CVD in HIV patients (Shah *et al.,* 2015). In addition to immunological defects and metabolic disorders, the adverse effects of antiretroviral therapy have become a particular concern within factors that may potentially contribute to HIV-related CVD (de Gaetano *et al.,* 2004). Importantly, both arterial and small-vessel vasculopathy are indicated, in which endothelial dysfunction could be a major cause.

So far, a number of laboratory studies have revealed that NRTIs have a detrimental effect in the development of atherosclerosis, a major aortic disease. The long-term administration of NRTIs significantly exacerbated the intima-media remodelling of the aorta and carotid artery in mice, and this was associated with endothelial dysfunction (Roy *et al.,* 2002; Jiang *et al.,* 2009; 2010). Furthermore, mechanical investigations have shown that NRTIs cause mitochondrial dysfunction and oxidative stress in arterial endothelial cells (ECs) (Jiang *et al.,* 2007). However, a number of studies have reported that antiviral treatment in HIV-positive patients inhibited the occurrence and progression of Kaposi sarcoma, an AIDS-defining illness characterized by an abundant growth of immature microvessels originating from the lymphatic endothelium (Beckstead *et al.,* 1985) and mesenchymal–endothelial transitions (Gurzu *et al.,* 2013). These clinical cases suggest NRTIs can have potent effects on angiogenesis and lymphangiogenesis. Moreover, NHLBI of the NIH demonstrated a close correlation between antiviral treatment and endothelial dysfunction in HIV-positive patients. Because angiogenic capability is one of the basic functions of endothelial cells, this characteristic is an indicator of the interference of NRTIs in angiogenesis. Therefore, the ARTs used to treat HIV could be potent anti-angiogenic molecules. However, the biological effect of ART on the growth of vasculature remains elusive.

The human vascular system comprises blood vessels and lymphatic vessels, which form diffused networks among most cells of the body for material exchange, signal communication and homeostasis maintenance in the healthy organism (McColl *et al.,* 2004; Adams and Alitalo, 2007; Wang and Oliver, 2010b; Choi *et al.,* 2012). The new vessel growth from pre-existing vessels of these two vascular systems plays a central role in tissue morphogenesis during development and adult repair, coordinating the proliferation, migration and adhesion of ECs under the control of angiogenic signalling (Eichmann and Simons, 2012; Marcelo *et al.,* 2013). VEGFs, FGFs and their receptors are key regulators in angiogenesis and lymphangiogenesis *via* typical **receptor tyrosine kinase** (**RTK**) pathways; **VEGF-A**/**VEGFR2** and **bFGF**/ **FGFR1** are critical mediators in angiogenesis, while **VEGF-C**/**VEGFR3** is a key regulator of lymphatic angiogenesis (Horowitz and Simons, 2008; Wang *et al.,* 2010a; Murakami *et al.,* 2011). Upon binding of these growth factor ligands, corresponding RTKs undergo dimerization, followed by intrinsic phosphorylation/activation and consequent internalization and endocytosis of receptor-ligand complexes for triggering signalling transduction (Lanahan *et al.,* 2010; Zhang *et al.,* 2013).

Unlike other cells, which contain large quantities of mitochondria that can satisfy the requirements for high energy, ECs obtain most of their energy through glycolytic metabolism rather than through mitochondria-dependent oxidative phosphorylation (Freed and Gutterman, 2013; Tang *et al.,* 2014). Although ECs only have relatively low levels of mitochondria, these endothelial mitochondria provide prominent signals for cellular responses (Tang *et al.,* 2014). To this end, mitochondria-derived ROS (mROS) is the major signal effector in ECs, and is regulated through the mitochondrial redox system, including the free radical scavengers recombinant human superoxide dismutase (MnSOD) and thioredoxin protein 2 (TRX2) (Bir *et al.,* 2012; Zhou *et al.,* 2013; Kim and Byzova, 2014). Under stress conditions, excessive amount of mROS are produced, which overturn the buffering capacity of the redox system, and thereby regulates the physiological functions of an organelle or causes cellular dysfunction (Bir *et al.,* 2012). Specifically, excessive mitochondrial ROS has been associated with a disruptive effect on RTK endocytosis, which is the upstream event required for RTK activation (Ushio-Fukai and Nakamura, 2008). Without endocytosis, the VEGF and FGF receptors cannot be further phosphorylated, and the signalling transductions are consequently suppressed.

In the present study, we investigated the effect of representative nucleoside/nucleotide analogues of NRTIs [tenofovir disoproxil fumarate (TDF), **azidothymidine (AZT)** and lamivudine (3TC)], an integral component of ART, on microvascular angiogenesis. We demonstrated that pharmaceutical doses of NRTIs profoundly inhibit vascular

angiogenesis and lymphangiogenesis both *in vivo* and *in vitro*. In addition, NRTI treatment induced mitochondrial oxidative stress and the subsequent impairment of RTK signalling in ECs. Specifically, NRTIs significantly restrained the endocytosis of RTKs into early endosomes and slightly affected their internalization.

Methods

Mice and diets

Animal studies are reported in compliance with the ARRIVE guidelines (Kilkenny *et al.*, 2010; McGrath and Lilley, 2015). All animal studies were approved by the Institutional Animal Care and Use Committee of Zhejiang University and adhered to the Guide for the Care and Use of Laboratory Animals. Eight-week-old male C57BL/6 mice (18–20 g) were purchased from Slac Laboratory Animal (Shanghai, China). The mice were acclimatized to the room for 1 week after arrival and maintained on a normal 12 h light–dark cycle. The mice were housed in conventional cages (six animals per cage) with free access to standard pellet diet and water. They were kept in specific pathogen-free conditions: temperature $24 \pm 2°C$, relative humidity 60–70%. Standard wood chips for mice were used as bedding material. The mice were randomly separated into two groups, which were administered distilled H_2O (control) or TDF (50 mg·kg^{-1}) by oral gavage for five consecutive days to ensure that serum concentrations were maintained above those needed to achieve therapeutic effects in humans (Jiang *et al.,* 2009; Jiang *et al.,* 2010). For each group, a cage was randomly selected from the pool of cages. The experimenters were blinded to the animal treatment, histological analyses and the data analyses. For the angiogenesis/lymphangiogenesis assays, the mice were anaesthetized with ketamine (200 mg·kg^{-1}) and xylazine (10 mg·kg^{-1}) through an i.p. injection. Anaesthesia was monitored using toe pinching. After the experiments, the mice were killed by cervical dislocation.

Mouse ear angiogenesis/lymphangiogenesis assay

Adenoviruses encoding VEGF-A$_{164}$ (1×10^9 pfu), bFGF (1×10^9 pfu), VEGF-C (1×10^9 pfu) or β-gal control (1×10^9 pfu) were injected, i.d., into mouse ear skin. Ten days later, the mice were killed, and the ears were photographed using a stereomicroscope. The mouse ears were subsequently fixed overnight in 4% paraformaldehyde at 4°C. The ears were washed three times with 1× PBS for 1 h and stained with anti-mouse CD31 (rat polyclonal, 10 μg·mL^{-1}; BD Pharmingen, San Diego, CA, USA) or LYVE-1 antibody (goat polyclonal, 10 μg·mL^{-1}; R&D, Minneapolis, MN, USA) diluted at 4°C for 24 h. The ears were subsequently washed three times with 1× PBS for 1 h followed by Alexa Fluor 488- or 594-conjugated secondary antibody (donkey polyclonal, 5-μg·mL^{-1}; Molecular Probes) at 4°C for another 24 h. The coverslips were mounted onto slides using Vectashield mounting medium (Vector Laboratories, CA, USA). Images were obtained using a Nikon fluorescence microscope (Tokyo, Japan) and analysed using Nikon NIS-Elements software. Quantitative analyses were conducted blindly.

In vivo Matrigel plug assay

Growth factor-reduced Matrigel (BD Biosciences) was premixed with murine VEGF-A$_{164}$ (50 ng·mL^{-1}), murine bFGF (100 ng·mL^{-1}) or murine VEGF-C (100 ng·mL^{-1}) and heparin (20 U·mL^{-1}). Recombinant murine VEGF and murine bFGF were purchased from Peprotech (Rocky Hill, NJ, USA). Murine VEGF-C was obtained from Sigma-Aldrich (St. Louis, MO, USA), and 100 μL of the samples was injected s.c. into 8-week-old mice. Two weeks later, the mice were killed, and the plugs were removed and imaged. Subsequently, 5 μm serial sections were cut from frozen, optimal cutting temperature compound-embedded plugs and mounted onto pre-cleaned glass slides. Prior to staining, the slides were placed at room temperature for half an hour and fixed in $-20°C$ acetone for 10 min, rinsed three times in PBS for 15 min and subsequently blocked in 10% normal horse serum for 1 h at room temperature. The slides were incubated overnight using anti-mouse CD31 antibody (rat polyclonal, 10 μg·mL^{-1}; BD Pharmingen) or LYVE-1 antibody (goat polyclonal, 10 μg·mL^{-1}; R&D) at 4°C for 24 h. The sections were subsequently washed with 1× PBS for half an hour, followed by Alexa Fluor 488- or 594-conjugated secondary antibody (donkey polyclonal, 5 μg·mL^{-1}, Molecular Probes, Eugene, OR, USA) at 4°C for 24 h. The coverslips were mounted onto slides using Vectashield mounting medium, and images were captured using a Nikon fluorescence microscope (Tokyo, Japan). The images were analysed using Nikon NIS-Elements software. Quantitative analyses were conducted blindly.

Cell culture

HUVECs and human dermal microvascular endothelial cells (HMVECs) were purchased from Lonza (Allendale, NJ, USA) and cultured with endothelial cell growth medium (EGM)-2 and EGM-2 MV (Lonza) respectively. Human dermal lymphatic endothelial cells (HDLECs) were purchased from PromoCell (Heidelberg, German) and cultured with endothelial cell growth medium MV-2 (PromoCell). Only cells from passages 3–8 were used for experiments. The 10 μM doses of drugs were carefully selected according to the International US AIDS Panel, and the average plasma drug concentrations were as previously reported (Chittick *et al.*, 2006; Jiang *et al.*, 2007; Xue *et al.*, 2013). For all *in vitro* experiments, the cells were treated with drugs for 48 h prior to testing. All cell lines were cultured at 37°C in 5% CO_2. For treatment with different growth factors, the cells were serum starved overnight and treated with VEGF-A$_{165}$ (50 ng·mL^{-1}), bFGF (100 ng·mL^{-1}), or VEGF-C (100 ng·mL^{-1}) for various times. Recombinant human VEGF-A$_{165}$, human bFGF and human VEGF-C were from Peprotech. Manganese (III) tetrakis (N-methyl-2-pyridyl) porphyrin (MnTMPyP) pentachloride was purchased from ApexBio (Houston, TX, USA).

In vitro EC migration and tube formation assays

Monolayer EC migration. For monolayer migration, ECs were seeded onto 12-well tissue culture plates and grown to confluence. The next day, control or NRTI-treated ECs were subjected to a 'wound healing' assay with a 200 μL plastic pipette tip. EC migration in the culture was determined by measuring wound areas in cell monolayers. Cells were dyed,

after 48 h, using 0.2% crystal violet (Sigma-Aldrich) dissolved in PBS containing 10% ethanol. Images were captured using a Nikon microscope, and wound healing (% closure) was subsequently measured and analysed.

EC transwell migration assay.   Cell migration was examined using a transwell fitted with an 8 μm pore size polycarbonate filters (Corning, NY, USA). Briefly, the lower chambers were filled with EGM-2 (Lonza), and 1×10^5 control or NRTI-treated ECs suspended in EBM-2 were added into each upper chamber. The cells were subsequently cultured for 8 h at 37°C in the presence of 5% CO_2 in a humidified incubator. Cells that did not migrate through the filters were removed with cotton swabs, and cells that migrated to the lower surfaces of the filters were stained for 15 min with 0.2% crystal violet in 10% ethanol. The chambers were washed thoroughly in a water reservoir, and the interior was dried with cotton swabs. Cells on the lower surfaces of the filters were counted under a microscope.

EC tube formation assay.   Control or NRTI-treated ECs were plated onto solidified Matrigel (Corning)-coated 48-well plates at 1×10^4 cells per well in EGM-2 for 6 h at 37°C in the presence of 5% CO_2 in a humidified incubator. Images of the formation of tube or vascular-like structures were observed using a Nikon inverted phase contrast microscope, and tube formation was quantified by measuring the number of branches produced.

Apoptosis assay

Alexa Fluor 488 annexin V/Dead Cell Apoptosis Kit (Sigma-Aldrich) was used to measure cell apoptosis. Control or NRTI-treated ECs were incubated with reagents from the kit according to the manufacturer's instructions, followed by flow cytometry analysis. The rate of apoptosis was expressed as a percentage of apoptotic cells relative to the total number of cells per condition. Cells treated with staurosporine (1 mM final concentration) for 3 h were used as the positive control.

Cell lysis and Western blot analysis

To obtain cell lysates, the cells were washed with cold PBS and lysed for 10 min on ice in a RIPA lysis buffer (50 mM Tris–HCl, pH 7.4, 150 mM NaCl, 1% NP-40, 0.5% sodium deoxycholate, 0.1% SDS) containing protease inhibitor mixture (Roche, Basel, Switzerland) and phosphatase inhibitor mixture (Roche). The cell lysates were subsequently centrifuged at $14\,000 \times g$ at 4°C for 15 min, and the supernatants were immediately used for immunoblotting analyses. The complexes were loaded in 8–10% polyacrylamide gels and transferred onto PVDF membranes. The membranes were then blocked with 5% skimmed milk diluted in PBS containing 0.05% Tween 20 for 1 h and subsequently immunoblotted at 4°C overnight with specified primary antibodies: phospho-VEGFR2 (Tyr[1059]) (rabbit polyclonal, 1 μg·mL^{-1}; Cell Signaling Technology, Beverly, MA, USA), VEGFR2 (rabbit polyclonal, 1 μg·mL^{-1}; Cell Signaling Technology), phospho-FGFR1 (mouse polyclonal, 1 μg·mL^{-1}; Cell Signaling Technology), FGFR1 (rabbit polyclonal, 1 μg·mL^{-1}; Cell Signaling Technology), VEGFR-3 (rabbit polyclonal, 1 μg·mL^{-1}; Cell Signaling Technology), phospho-PLCγ (pY783) (rabbit polyclonal, 1 μg·mL^{-1}; Cell Signaling

Technology), PLCγ (rabbit polyclonal, 1 μg·mL^{-1}; Cell Signaling Technology), phospho-Akt (Ser[473]) (rabbit polyclonal, 1 μg·mL^{-1}; Cell Signaling Technology), **Akt** (rabbit polyclonal, 1 μg·mL^{-1}; Cell Signaling Technology), phospho-FRS2.alpha; (rabbit polyclonal, 1 μg·mL^{-1}; Cell Signaling Technology), phospho-p44/42 MAPK (rabbit polyclonal, 1 μg·mL^{-1}; Cell Signaling Technology), cleaved **Notch1** (Val[1744]) (rabbit polyclonal, 1 μg·mL^{-1}; Cell Signaling Technology), HES1 (D6P2U) (rabbit polyclonal, 1 μg·mL^{-1}; Cell Signaling Technology), thioredoxin 2 (rabbit polyclonal, 1 μg·mL^{-1}; Cell Signaling Technology), ERK1 (K-23) (rabbit polyclonal, 2 μg·mL^{-1}; Santa Cruz Biotechnology, Santa Cruz, CA, USA), FRS2α (A-5) (rabbit polyclonal, 2 μg·mL^{-1}; Santa Cruz Biotechnology), phospho-VEGFR3 (Tyr[1230/1231]) antibody (rabbit polyclonal, 1 μg·mL^{-1}; Cell Application, San Diego, CA, USA), anti-catalase antibody (rabbit polyclonal, 1 μg·mL^{-1}; Abcam, Cambridge, MA, USA) and anti-MnSOD antibody (rabbit polyclonal, 1 μg·mL^{-1}; Millipore, Bedford, MD, USA). After being washed in PBS for 30 min, the membranes were incubated with relevant secondary antibodies at room temperature for 1 h. The membranes were treated with ECL reagents (Bio-Rad Laboratories, Hercules, CA, USA) prior to visualization using a FluoChem E Imager (Protein-simple, USA).

Matrigel lysis and Western blot analysis

Matrigel samples were obtained from mice *in vivo* and cut into pieces. The gel pieces were lysed using RIPA lysis buffer for 10 min on ice, followed by shearing with super sonication. Matrigel lysates were subsequently centrifuged at $14\,000 \times g$ at 4°C for 15 min. The supernatants were used for Western blot analyses.

Analysis of VEGFR2, FGFR1, VEGFR-3 internalization and surface expression using flow cytometry

Control or NRTI-treated ECs were serum-starved overnight, subsequently placed on ice and incubated with specified antibody for 30 min. PE anti-human CD309 (VEGFR2) and PE anti-human VEGFR-3 (FLT-4) were purchased from BioLegend (mouse polyclonal, 2.5 μg·mL^{-1}; San Diego, CA, USA), and FGFR1 antibody (N-term) was purchased from ABGENT (rabbit polyclonal, 2.5 μg·mL^{-1}; San Diego, CA, USA). Control or NRTI-treated ECs were subsequently stimulated with VEGF-A$_{165}$ (50 ng·mL^{-1}), bFGF (100 ng·mL^{-1}) or VEGF-C (100 ng·mL^{-1}) for pre-determined time intervals at 37°C and subsequently rinsed with ice-cold PBS or acidic wash (PBS, pH 2.5), respectively, to remove the remaining cell surface labelled receptors. The cells were subsequently treated with Accutase-Enzyme Cell Detachment Medium (eBioscience, San Diego, CA, USA), centrifuged and resuspended in PBS/1%BSA/1%formaldehyde, followed by flow cytometry analysis using a FACS-Calibur instrument (Becton Dickinson, Franklin Lakes, NJ, USA).

Colocalization of VEGFR2, FGFR1, VEGFR-3 and EEA1

Control or NRTI-treated ECs were grown on gelatin-coated glass coverslips (Thermo Fisher, USA) and starved overnight with 0.5% FBS. The cells were stimulated with VEGF-A$_{165}$

(50 ng·mL^{-1}), bFGF (200 ng·mL^{-1}) and VEGF-C (50 ng·mL^{-1}) and incubated for pre-determined time intervals at 37°C. The cells were subsequently washed with PBS and fixed with 4% PFA in PBS for 15 min at room temperature. The fixed cells were further incubated overnight with antibodies against VEGFR2 (rabbit polyclonal, 1 µg·mL^{-1}; Cell Signaling Technology), FGFR1 (rabbit polyclonal, 10 µg·mL^{-1}; Cell Signaling Technology) or VEGFR-3 (rabbit polyclonal, 1 µg·mL^{-1}; R&D), followed by Alexa Fluor 488- or 594-conjugated secondary antibody (donkey polyclonal, 5 µg·mL^{-1}; Molecular Probes). The next day, the cells were subsequently labelled with EEA1 antibody (mouse monoclonal, 1 µg·mL^{-1}; Abcam) overnight, followed by secondary antibody. The samples were observed through a laser-scanning confocal microscopy with an X63 objective.

Quantification of mtDNA copy number

RT-qPCR was performed with the All-in-one qPCR Mix (GeneCopoeia, Amaranth Drive Germantown, MD, USA) in triplicate on a 96-well plate with a CFX96 Connect Real-Time PCR Detection System (Bio-Rad). GAPDH served as an internal control. Primers with the following sense sequences were used:

5′CCC CAC ATT AGG CTT AAA AAC AGA T3′,
5′CCC CAC AAA CCC CAT TAC TAA ACC CA3′.

Determination of mROS production

MitoSOX (Invitrogen, Carlsbad, CA, USA) was used to determine mitochondria-derived ROS production according to the manufacturer's instructions. The images were observed using a Nikon fluorescence microscope and analysed using Nikon NIS-Elements software.

Statistical analysis

The data and statistical analysis comply with the recommendations on experimental design and analysis in pharmacology (Curtis *et al.*, 2015). Statistical analysis was performed using GraphPad Prism software. ImageJ, Photoshop CS and Illustrator CS software were used for image processing according to the general guidelines. All data, expressed as the means ± SEM, were analysed using Student's two-tailed *t*-test or one-way ANOVA. *P*-values < 0.05 were considered statistically significant.

Chemicals and reagents

TDF and 3TC were purchased from Energy Chemical (Shanghai, China). AZT was purchased from Sigma-Aldrich. Small amounts of TDF, AZT and 3TC were also obtained from the NIH AIDS Research and Reference Reagent Programme (Germantown, MD, USA).

Nomenclature of targets and ligands

Key protein targets and ligands in this article are hyperlinked to corresponding entries in http://www.guidetopharmacology.org, the common portal for data from the IUPHAR/BPS Guide to PHARMACOLOGY (Southan *et al.,* 2016), and are permanently archived in the Concise Guide to PHARMACOLOGY 2015/16 (Alexander *et al.,* 2015a,b,c).

Results

NRTIs weaken the angiogenic capability of ECs by disrupting cell proliferation and migration

To determine the effect of NRTIs on angiogenic cell growth, we employed primary cultured HMVECs and HUVECs in an *in vitro* model of angiogenesis and HDLECs in an *in vitro* model of lymphangiogenesis. To mimic ART administration, these ECs with pharmaceutical doses of representative NRTIs (TDF, AZT and 3TC). No induction of apoptosis was detected with all the three NRTIs in all the three cell lines (Figure 1A and Supporting Information Figure S1A). The growth of ECs was first examined using a monolayer 'wound healing' assay. NRTI treatment resulted in significantly slower wound closure compared to carrier control in all three types of EC growing in full medium (Figure 1 B–E and Supporting Information Figure S1B, C, *P* < 0.05). The closure of the wound within 48 h is attributed to two distinct cellular processes, proliferation and migration. Thus, we measured the effect of NRTIs on EC proliferation and migration separately. EC proliferation was measured using a CCK-8 assay and the cell growth curves indicated that NRTI treatment blunted the proliferation of the ECs (Figure 1F and Supporting Information Figure S1D, *P* < 0.05). Under the same conditions in full medium, using a transwell migration assay, it was observed that NTRI retarded the migratory capability of the cells (Figure 1G–J and Supporting Information Figure S1E–F, *P* < 0.05). Correspondingly, F-actin staining showed that the addition of NRTI destroyed the original organization of microfilaments, which are essential for EC movement (Supporting Information Figure S2). To further investigate the effect of NRTIs on the angiogenic ability of ECs, a tube formation assay was performed. Similar to the results obtained with the proliferation and migration analysis, NRTI-treated ECs barely formed hollow lumens and capillary-like structures, while control cells achieved typical capillary-like tube structures (Figure 1K–N and Supporting Information Figure S1G, H, *P* < 0.05). Taken together, these findings show that NRTIs specifically disrupt the migration capability of ECs and consequently cellular angiogenesis.

NRTIs block angiogenesis and lymphangiogenesis in vivo

The angiogenic assays *in vitro* involve multiple pro-angiogenic factors, which function distinctly in vascular network formation. At the physiological level, the expression of VEGF receptors (VEGFRs) is primarily confined to vascular ECs and lymphatic ECs; FGFR1 is highly expressed in vascular ECs. When new vessels start to grow, the tip cells at the angiogenic fronts migrate towards to the VEGF stimulus that activates the VEGF–VEGFR signalling pathway, leading to the promotion of angiogenesis. Inside the neovascular area, bFGF-activated FGFR signalling is a major force driving the proliferation and maturation of the endothelial network (Horowitz and Simons, 2008; Koch and Claesson-Welsh, 2012; Simons and Eichmann, 2015). Therefore, as VEGF-A, bFGF and VEGF-C are the most important pro-angiogenic factors, we employed them in endothelial angiogenic assays to investigate the effect of NRTIs
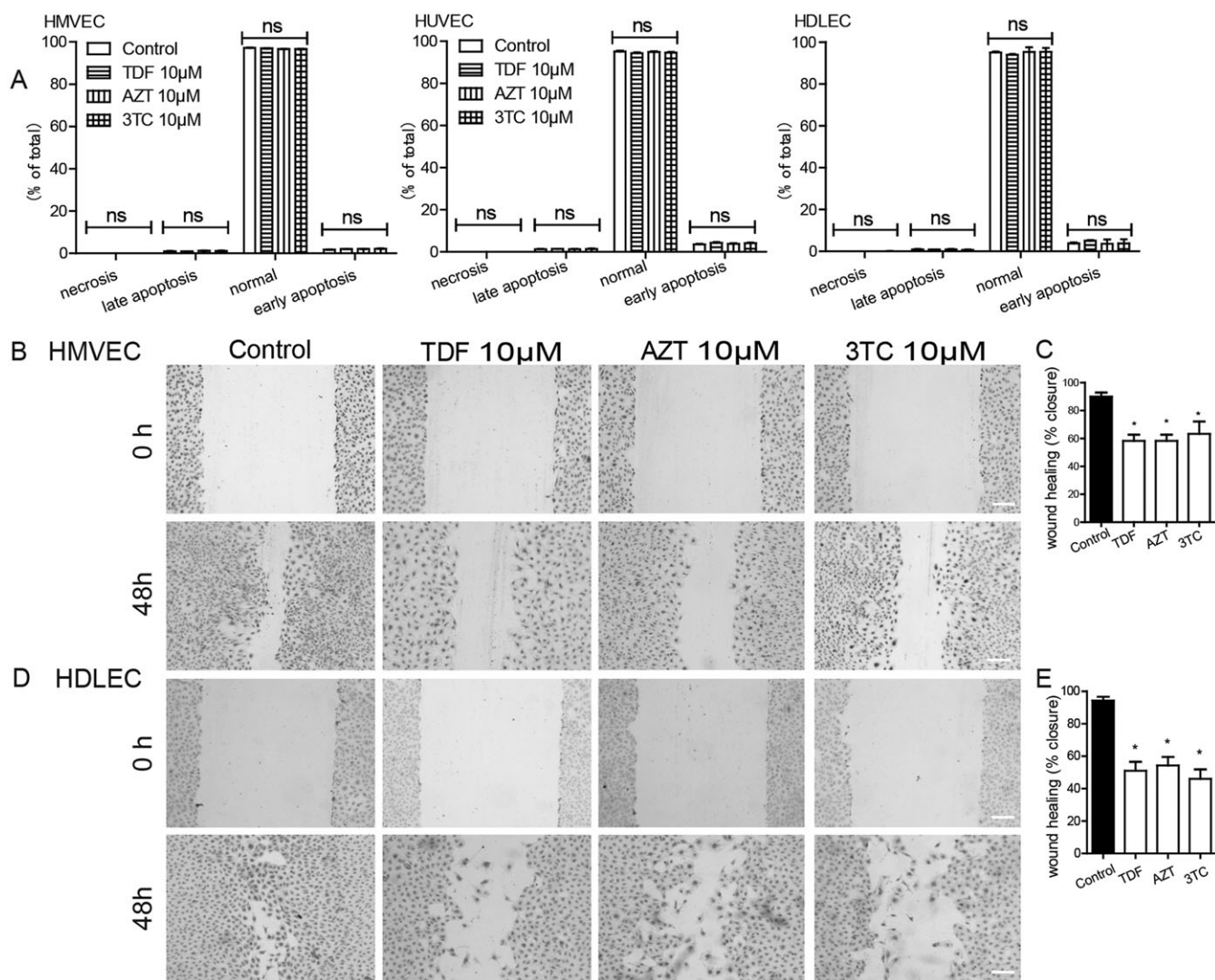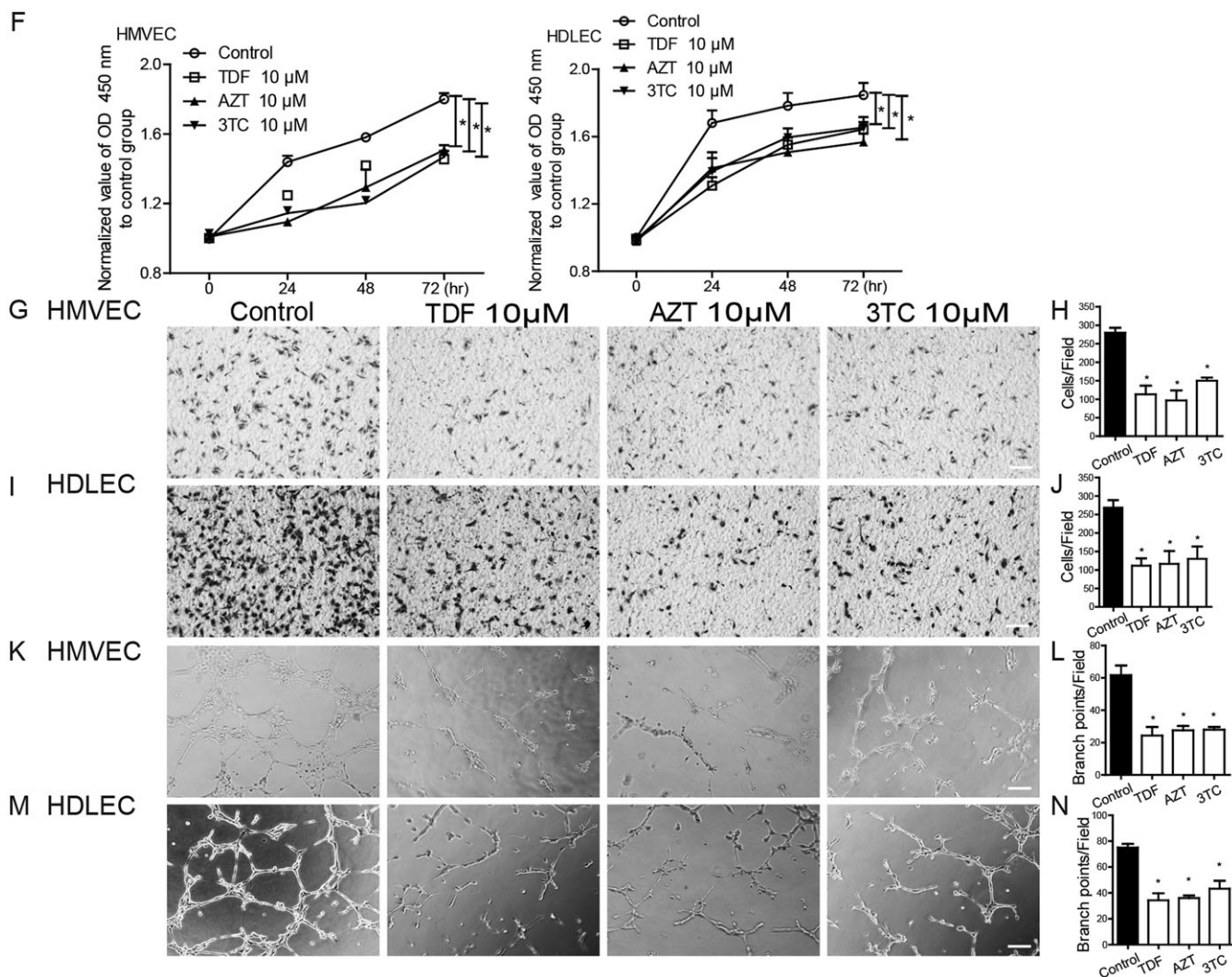
Figure 1

Effects of NRTI treatment on the proliferation, migration and tube formation of microvascular ECs and microlymphatic ECs. (A) After TDF, AZT or 3TC treatment for 48 h, HMVECs, HUVECs and HDLECs were stained with PI and annexin-V-FITC, followed by detection on a flow cytometer. The populations of early apoptotic cells (annexin-V positive/PI negative) and late apoptotic cells (PI positive) were evaluated as a % of total cells. Data represent the means ± SEM based on five independent experiments. ns, not significant. (B–E) After TDF, AZT or 3TC treatment for 48 h, confluent monolayers of ECs were subjected to a wound healing assay. Representative images of HMVECs and HDLECs are shown in (B) and (D) respectively. Wound closure was quantified as % in (C) and (E). Data represent the means ± SEM based on five independent experiments. Scale bar, 200 μm. *$P < 0.05$ versus control. (F) After TDF, AZT or 3TC treatment for 48 h, cell proliferation of HMVECs and HDLECs was measured by Cell Counting Kit-8 assay. Data represent the means ± SEM from triplicates in each group from five independent experiments. *$P < 0.05$ versus control. (G–J) After TDF, AZT or 3TC treatment for 48 h, HMVECs and HDLECs were subjected to a transwell migration assay. Eight hours later, cells on the reverse side of the membrane were stained with crystal violet. Representative images are shown in (G) and (I). Migratory cells were quantified in (H) and (J). Data represent the means ± SEM from duplicates (six different areas in each well) from five independent experiments. Scale bar, 100 μm. *$P < 0.05$ versus control. (K–N) Tube formation assay in Matrigel. After TDF, AZT or 3TC treatment for 48 h, HMVECs or HDLECs were seeded onto Matrigel for 6 h, and representative images are shown in (K) and (M). Branch points were quantified in (L) and (N). Data represent the means ± SEM from triplicates in each group from five independent experiments. Scale bar represents 100 μm. *$P < 0.05$ versus control; ns, not significant.

on angiogenesis and lymphangiogenesis. To directly assess the effect of NRTIs on vascular responses to these pro-angiogenic growth factors *in vivo*, we examined angiogenesis and lymphangiogenesis in the ear and implanted Matrigel plugs in mice using a representative NRTI, TDF. For the ear angiogenesis model, an adenovirus encoding VEGF-A$_{164}$, bFGF, VEGF-C or β-gal was injected i.d. into mice ears. The angiogenesis/lymphangiogenesis induced by

a single growth factor was determined by stereomicroscopy (Figure 2A, D, G). Ear vascular or lymphatic vessels were also visualized using whole-mount immunofluorescent staining with anti-CD31 or anti-LYVE-I antibody (Figure 2B, E, H with quantifications in Figure 2C, F, I). In these assays, injection of Ad-VEGF-A$_{164}$ or Ad-bFGF led to profound local angiogenesis and injection of Ad-VEGF-C resulted in an intense local area of lymphangiogenesis
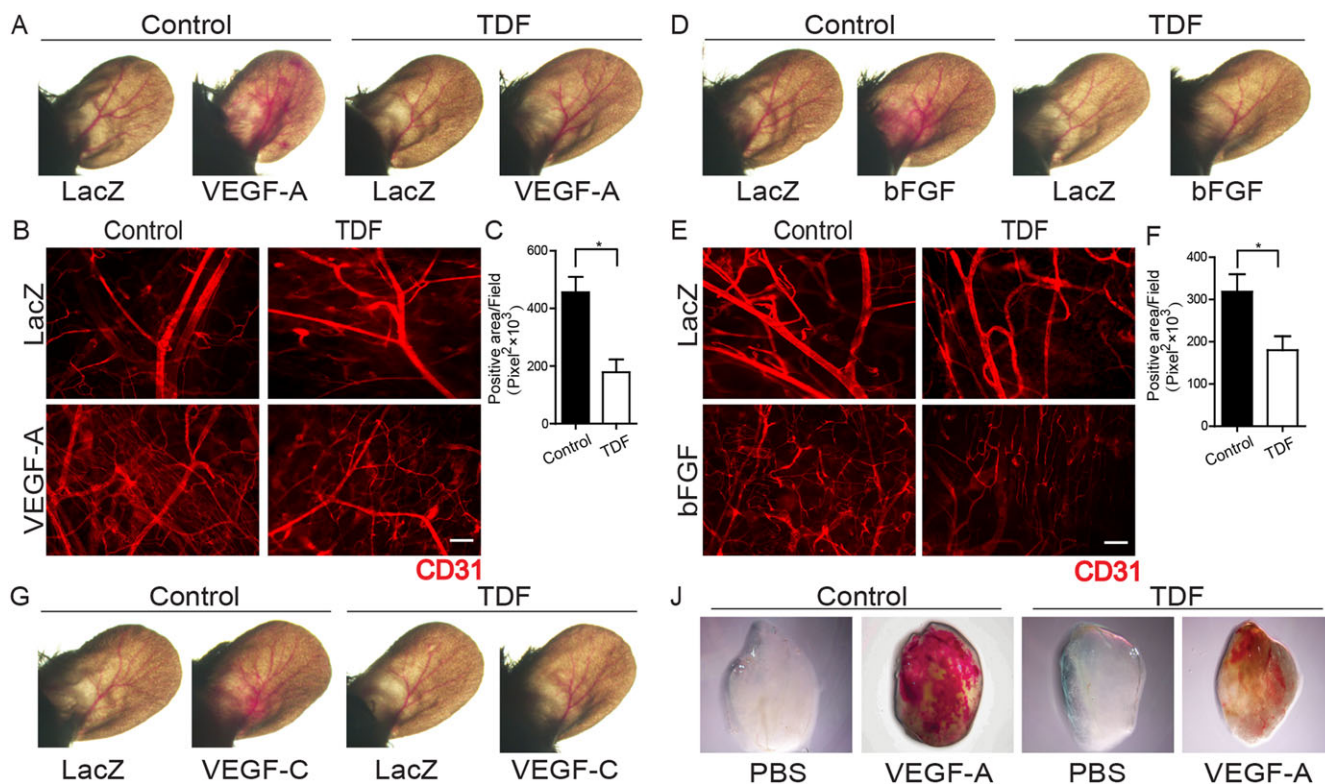
Figure 1

(Continued)

in control animals. However, the responses to these three growth factors were significantly reduced in animals after TDF administration ($P < 0.05$, $n = 6$). Consistently, the angiogenesis/lymphangiogenesis responses in implanted Matrigel plugs premixed with murine VEGF-A$_{164}$, bFGF or VEGF-C were dramatically decreased in the TDF-treated groups (Figure 2J, K, M, N, P, Q with quantifications in Figure 2L, O, R, $P < 0.05$, $n = 6$), AZT-treated groups (Supporting Information Figure S3A, B, D, E, G, H with quantifications in Supporting Information Figure S3C, F, I, $P < 0.05$, $n = 6$) and 3TC-treated groups (Supporting Information Figure S3J, K, M, N, P, Q with quantifications in Supporting Information Figure S3L, O, R, $P < 0.05$, $n = 6$).

NRTI treatment suppresses RTK signalling in ECs

In vascular ECs, the corresponding receptors for VEGF-A, bFGF and VEGF-C are from the same group of RTKs, which function as principal regulators of EC growth and angiogenesis (McColl *et al.,* 2004; Wang *et al.,* 2010a). Thereby, we reasoned that the mechanism by which NTRIs inhibit angiogenesis and lymphangiogenesis involves the interference of RTK signalling in ECs. To this end, primary cultured vascular ECs were treated with VEGF-A, bFGF or VEGF-C, and activation of RTK pathways was determined through Western blotting with phospho-specific antibodies. In HMVECs, VEGF-A induced the phosphorylation of VEGFR2 and its downstream effector Akt, PLCγ and **ERK1/2**. Consistent with the angiogenesis assays, VEGFR2-mediated activation of PLCγ, ERK1/2 and Akt was substantially weakened in NRTI-treated ECs (Figure 3A–C, $P < 0.05$, $n = 5$). Similar results were obtained using HUVECs (Supporting Information Figure S4A–C, $P < 0.05$, $n = 5$). In addition, in untreated cells bFGF induced the phosphorylation of FGFR1, its adaptor FRS2α, and the downstream Akt and ERK1/2, whereas in the presence of NRTIs these effects of bFGF were blocked in both HMVECs (Figure 3D–F, $P < 0.05$, $n = 5$) and HUVECs

Figure 2

Impaired angiogenesis and lymphangiogenesis in TDF-treated mice. (A–I) After receiving distilled water (control) or TDF (50 mg·kg^{-1}) for 5 days, C57BL/6 mice were injected with 1×109 pfu of adenovirus encoding VEGF-A164, bFGF, VEGF-C or β-gal (Ad-VEGF-A164, Ad-bFGF, Ad-VEGF-C or Ad-LacZ) i.d. into the ears. On day 10, angiogenesis induced by VEGF-A164 and bFGF and lymphangiogenesis induced by VEGF-C were recorded using stereomicroscopy, and representative images of the ears are shown in (A), (D) and (G) respectively. Ear vascular and lymphatic vessels were assessed through whole-mount staining of mouse ears with anti-CD31 and anti-LYVE-I, respectively, using immunofluorescence microscopy. Representative images of the ears with Ad-VEGF-A164, Ad-bFGF and Ad-VEGF-C are shown in (B), (E) and (H) respectively. Positive areas of new microvessels was quantified in (C), (F) and (I). Data represent the means ± SEM; $n = 6$ mice per group. Scale bar represents 100 μm. *$P < 0.05$ versus control. (J–R) Matrigel mixed with either PBS (control), VEGF-A164 (50 ng·mL^{-1}), bFGF (100 ng·mL^{-1}) or VEGF-C (100 ng·mL^{-1}) was placed subcutaneously in C57BL/6 mice previously fed with distilled water (control), TDF (50 mg·kg^{-1}) for 5 days. On day 10, Matrigel plugs were harvested and recorded using stereomicroscopy. Representative images of plugs are shown in panels (J), (M) and (P). Matrigel plugs were subsequently sectioned, and vascular and lymphatic vessels were subsequently assessed using immunofluorescence staining with anti-CD31 and anti-LYVE-I respectively. Representative images of plugs with Ad-VEGF-A164, Ad-bFGF and Ad-VEGF-C are shown in panels (K), (N) and (Q) respectively. Positive areas of new microvessels were quantified in L, O and R. Data represent the means ± SEM; $n = 6$ mice per group. Scale bar represents 50 μm. *$P < 0.05$ versus control.

(Supporting Information Figure S4D–F, $P < 0.05$, $n = 5$). For lymphangiogenesis, we examined the VEGF-C-activated VEGFR3 pathway in HDLECs and observed that NRTIs consistently suppressed VEGFR3 activation and its downstream effectors (Figure 3G–I, $P < 0.05$, $n = 5$). Notably, we observed that AZT altered the total expression of VEGFR2 and FGFR1 (Figure 3B, E and Supporting Information Figure S4B, E second rows). The maturation and signal transduction of VEGFR2 and FGFR1 depend on the N-glycosylation of these RTK receptors (Feige and Baird, 1988; Takahashi and Shibuya, 1997; Shen *et al.*, 1998; Duchesne *et al.*, 2006). Further immunoblot analyses of HMVECs treated with AZT or tunicamycin, an antibiotic that specifically inhibits the N-glycosylation of proteins, were performed. AZT treatment reduced the bands of VEGFR2 and FGFR1 to a single band, whose size coincides with that of the upper band observed in the presence of

tunicamycin (Supporting Information Figure S5A, B). Therefore, AZT blocks the maturation of proteins by partially decreasing their glycosylation. However, NRTIs had little effect on endothelial Notch1 signalling, the other classical membrane receptor pathway controlling EC growth. The expression of Notch 1 and its downstream Hes 1 detected in HMVECs and HUVECs was similar with or without NRTI treatment (Figure 3J,K and Supporting Information Figure S4G). Thus, NRTI treatment dampens angiogenic/lymphangiogenic activity by selectively targeting RTK pathways in vascular ECs. The activation of RTKs and their signature downstream molecules were further determined in the Matrigel plugs using Western blotting. Consistent with the results in cultured ECs, TDF significantly blocked RTK signalling *in vivo* (Supporting Information Figure S4H–J).
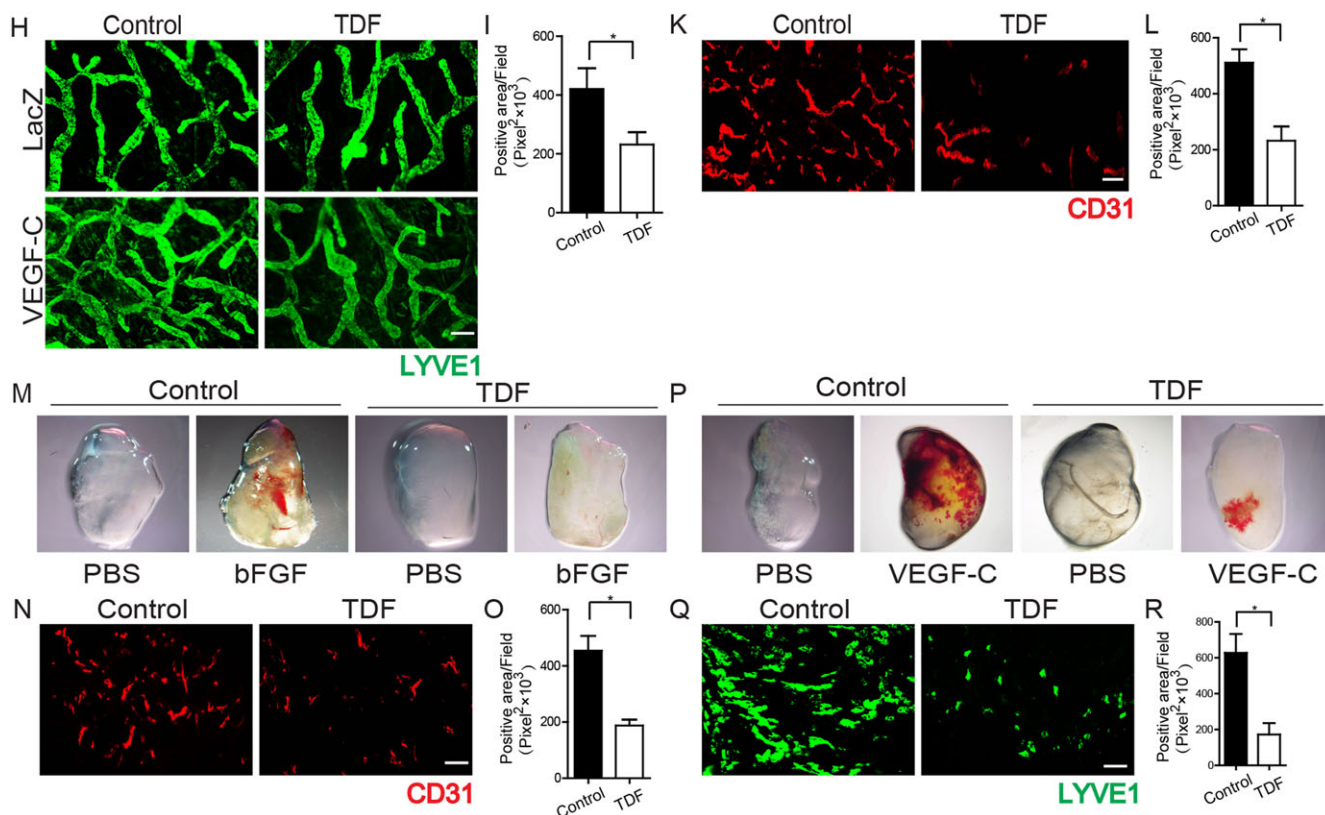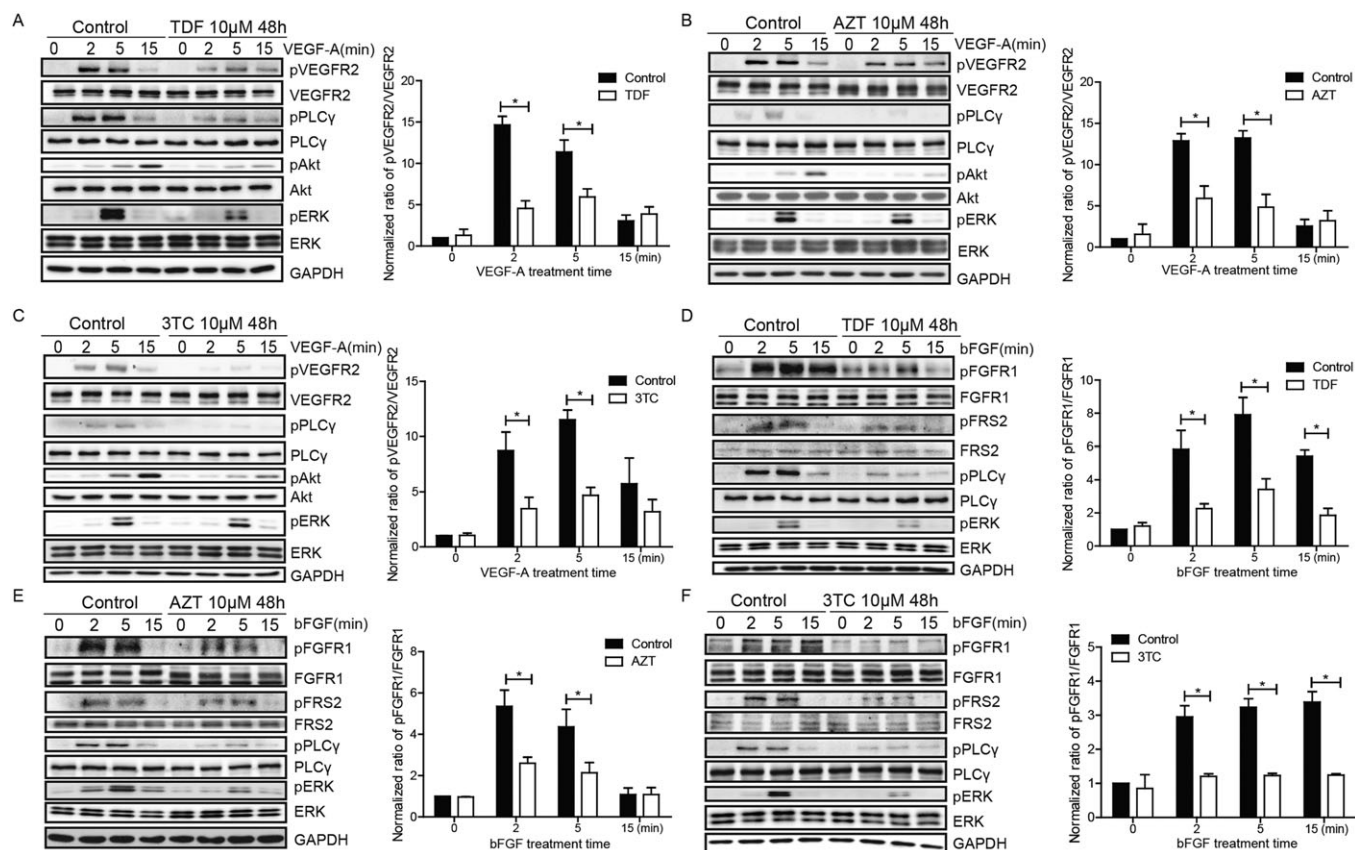
Figure 2
(Continued)

NRTIs restrain the internalization of RTKs or their endocytosis into early endosomes in ECs

To further investigate the mechanism of the inhibitory effects of NRTIs on endothelial RTK pathways, we examined membrane receptor internalization and endocytosis, two critical steps for the activation of RTK signalling. In HMVECs, flow cytometry analyses demonstrated that VEGF-A-induced VEGFR2 uptake was not affected in the presence of TDF and 3TC (Figure 4A with quantifications in Figure 4C). However, AZT treatment promoted VEGFR2 internalization in HMVECs, even without ligand stimulation (Figure 4B with quantifications in Figure 4C, $P < 0.05$, $n = 5$), and a similar pattern also applied for FGFR1 and VEGFR3 (Figure 4D, E, G, H with quantifications in Figure 4F, I). Similar results were also observed in HUVECs (Supporting Information Figure S6A, B, D, E with quantifications in Supporting Information Figure S6C, F). Notably, AZT treatment increased both total and internalized RTK levels in the absence of ligand stimulation, which resulted in decreased FGFR1 surface expression; whereas a downward trend was also observed for VEGFR2 and VEGFR3 (Supporting Information Figure S7A–F). Therefore, AZT may block RTK signalling in angiogenesis by disturbing both RTK surface expression and internalization. The effect of TDF and 3TC on RTK intracellular trafficking, transportation of VEGFR2, FGFR1 and VEGFR3 into early endosomes was determined using immunofluorescence microscopy. Upon stimulation by growth factors, RTKs are extensively translocated into EEA1-labelled endosomes in control HMVECs, HUVECs or HDLECs, but the endocytosis of internalized RTK was substantially retarded by either TDF or 3TC (Figure 4J, L, N and Supporting Information Figure S6G, I with quantifications in Figure 4K, M, O and Supporting Information Figure S6H, J, $P < 0.05$, $n = 5$).

NRTIs affect angiogenesis/lymphangiogenesis by causing mitochondrial oxidative stress

To examine the correlation between cellular stress induced by NRTIs and their inhibitory effects on angiogenesis and lymphangiogenesis, we determined the mitochondrial function, the main end target of antiviral medicine treatment, in NRTI-treated microvascular ECs. Mitochondrial DNA copy number was measured as a parameter of mitochondrial function. After 48 h, NRTIs markedly reduced mitochondrial DNA content (Figure 5A, B and Supporting Information Figure S8A), indicating an impairment in mitochondrial gene stability and biogenesis. As expected, excessive mROS production was detected along with this mitochondrial dysfunction in ECs (Figure 5C, D and Supporting Information Figure S8B, $P < 0.05$, $n = 5$). The imbalance of mitochondrial redox was also characterized by changes in the expression of mitochondrial antioxidant catalases. To this end, the expressions of MnSOD, TRX2 and catalase were examined using Western blotting.

Figure 3

NRTI treatment blocks RTK pathways in HMVECs and HDLECs. (A–C) Control and NRTI-treated HMVECs were serum-starved overnight and treated with VEGF-A165 (50 ng·mL^{-1}) as indicated. Cell lysates were blotted with antibodies against p-VEGFR2, VEGFR2, p-PLCγ, PLCγ, p-Akt, Akt, p-ERK or ERK respectively. (D–F) Control and NRTI-treated HMVECs were serum-starved overnight and treated with bFGF (100 ng·mL^{-1}) as indicated. Cell lysates were blotted with antibodies against p-FGFR1, FGFR1, p-PLCγ, PLCγ, p-FRS2, FRS2, p-Akt, Akt, p-ERK or ERK respectively. (G–I) Control and NRTI-treated HDLECs were serum-starved overnight and treated with VEGF-C (100 ng·mL^{-1}) as indicated. Cell lysates were blotted with antibodies against p-VEGFR3, VEGFR3, p-Akt, Akt, p-ERK or ERK respectively. (J) Cell lysates of control and NRTI-treated HMVECs were blotted with Notch1 or Hes1 antibody. (K) Cell lysates of control and NRTI-treated HDLECs were blotted with Notch1 or Hes1 antibody. Representative images in (A–K) were obtained from five independent experiments. Data represent the means ± SEM of five independent experiments determined using densitometry relative to the corresponding total proteins in (A–I) and relative to GAPDH in (J–K). *$P < 0.05$ versus control; ns, not significant.

Upon treatment with NRTIs, the level of MnSOD was elevated and TRX2 was slightly increased, while little change in catalase was detected (Figure 5E, F and Supporting Information Figure S8C, $P < 0.05$, $n = 5$). Importantly, the exogenous addition of the MnSOD mimic MnTMPyP restored the angiogenic and lymphangiogenic ability of ECs subjected to NRTI-induced impairments. In the presence of MnTMPyP, NRTI-treated ECs demonstrated an improved angiogenic/lymphangiogenic capability, evidenced by enhanced tube formation (Figure 6A, C with quantifications in Figure 6B, D and Supporting Information Figure S9A with quantifications in Supporting Information Figure S9B, $P < 0.05$, $n = 5$). Concomitantly, MnTMPyP reactivated the endothelial VEGFR2, FGFR1 and VEGFR3 signalling, which was retarded by TDF (Figure 6E–G and Supporting Information Figure S9C, D, $P < 0.05$, $n = 5$) and 3TC (Figure 6H–J, $P < 0.05$, $n = 5$). Therefore, ROS derived from dysfunctional mitochondria is the critical mediator involved in NRTI-induced inhibition of angiogenesis and lymphangiogenesis.

Discussion

The correlation between ART and cardiovascular disorders has only been partly explained (Jiang *et al.,* 2007; 2010; Reyskens and Essop, 2014); however, the precise role of ART remains largely unknown. In the present study, the effect of NRTIs on vascular growth was first evaluated in primary cultures of human microvascular or microlymphatic ECs. Vascular ECs showed a normal survival status under NRTI treatment at the normal pharmacological dose. However, NRTIs suppressed vascular tube formation by arresting the proliferation and migration of ECs. This negative effect of NRTIs on neovascularization was further confirmed using *in vivo* models. VEGF-A, bFGF and VEGF-C, the typical vascular growth factors responsible for different stages of vascular growth, were administered to induce angiogenesis and lymphangiogenesis in the Matrigel plugs or ears of mice. The results showed that pretreatment with NRTIs markedly limited the formation of vascular networks. Furthermore,
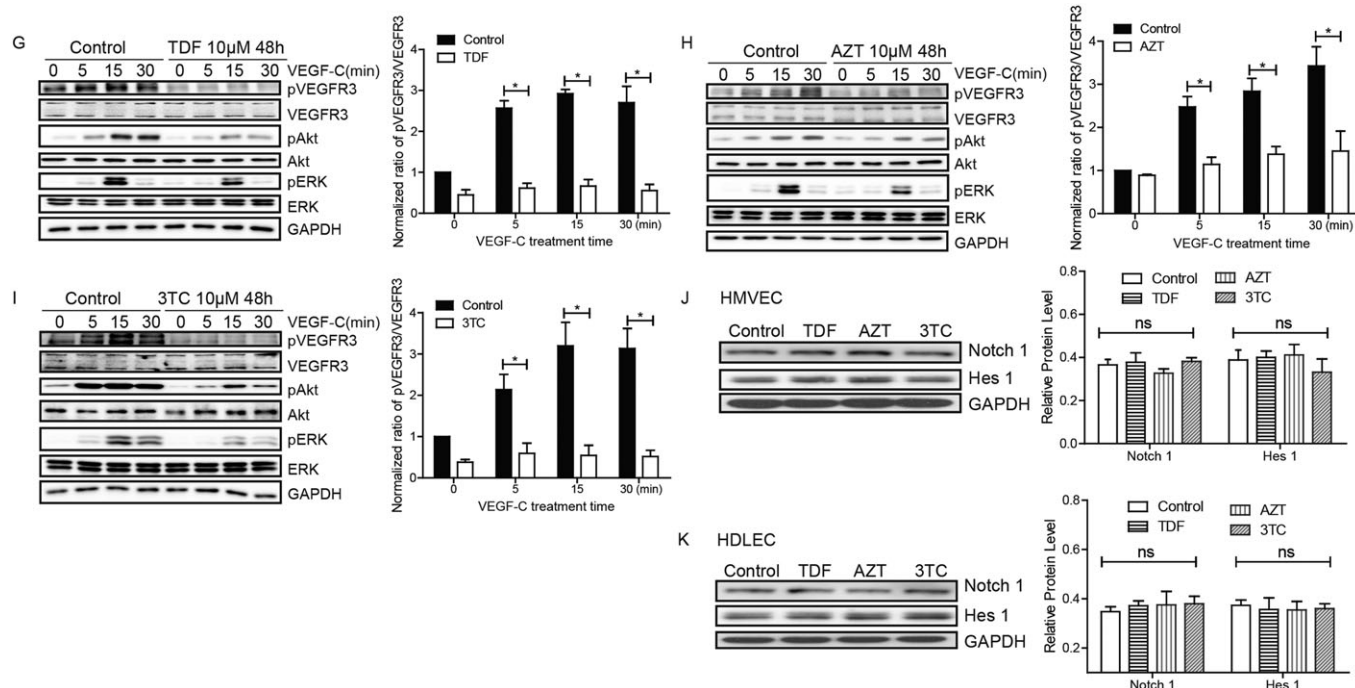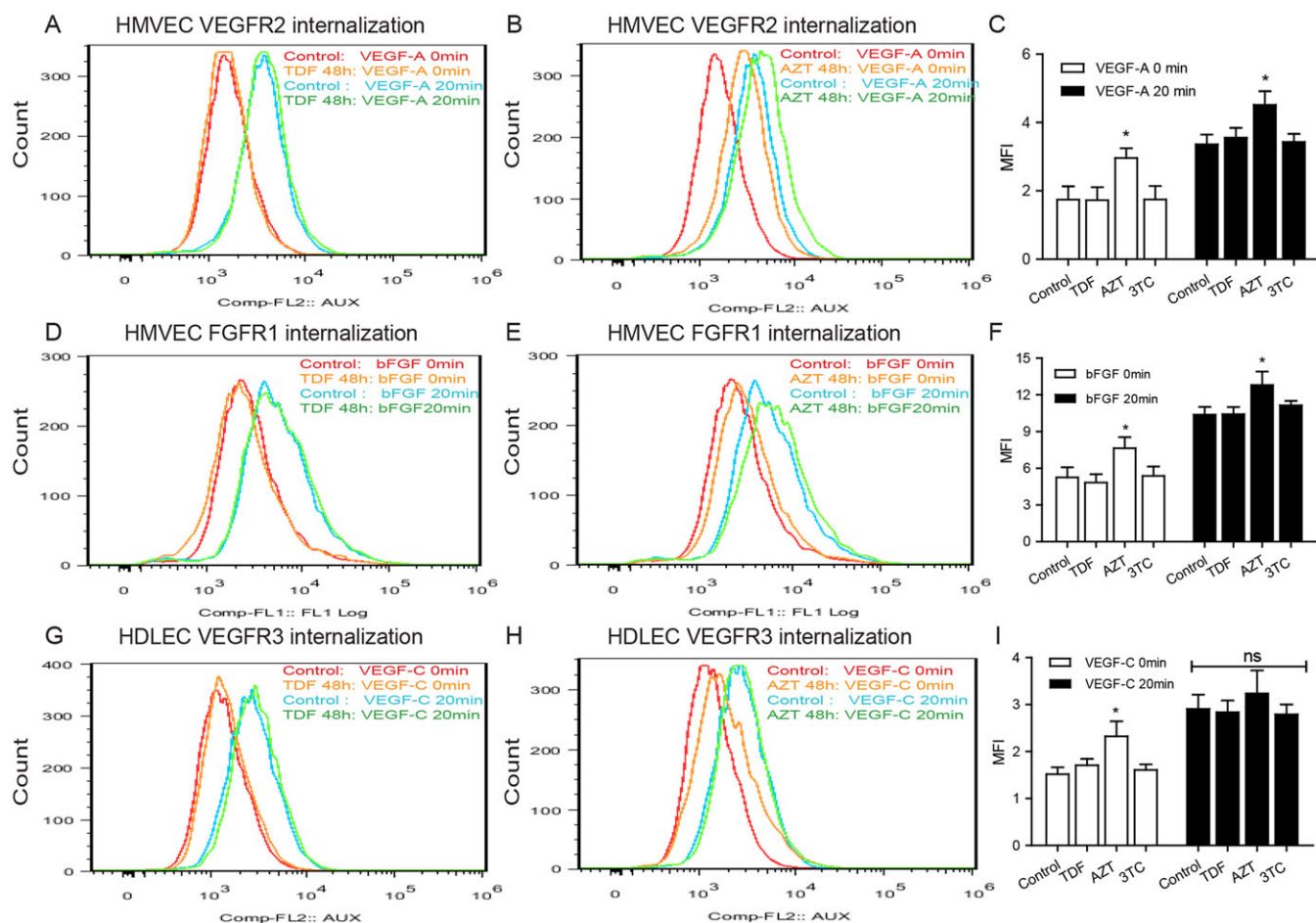
Figure 3

(Continued)

mechanistic studies demonstrated that NRTIs dampened vascular growth factor-mediated angiogenic/lymphangiogenic signalling transduction in ECs. Therefore, the present study reveals that NRTIs have a direct inhibitory effect on endothelial angiogenesis and lymphangiogenesis.

VEGF and FGF are critical factors in the regulation of angiogenesis and lymphangiogenesis, which function by activating corresponding RTK receptors on ECs (McColl *et al.,* 2004; Yang *et al.,* 2008; Lanahan *et al.,* 2010; Eichmann and Simons, 2012). VEGFR2 and FGFR are implicated in growth and haemostasis, respectively, in most aspects of normal and pathological vascular-endothelial-cell biology, whereas VEGFR3 is critical for lymphatic-endothelial-cell growth and function. In the present study, the NRTIs impaired the neovascularization induced by each growth factor (VEGF and bFGF) alone, indicating that NRTIs have an effect on RTK activation. Indeed, NRTIs suppressed RTK signal transduction both *in vitro* and *in vivo.* Therein, these results may reveal a molecular mechanism through which NRTIs retard angiogenesis. Furthermore, NRTIs had widespread effects on the functioning of RTKs. We observed that NRTIs not only inhibited VEGF-A/VEGFR2 and bFGF/FGFR1 signalling in ECs, but also attenuated VEGF-C-induced lymphangiogenesis and angiogenesis *in vivo.* However, the decreased neovessel formation in Matrigel/ear with VEGF-C cannot be attributed to the block of lymphangiogenesis. Recent studies indicate that VEGFR2 and VEGFR3 interact to induce angiogenesis; the two RTK signalling factors have different functions (Benedito *et al.,* 2012; Zarkada *et al.,* 2015). Thus, NRTIs may affect the competitive interaction between VEGFR2 and VEGFR3 activation, leading to suppression of the VEGFR2 pathway in vascular angiogenesis.

Indeed, it is now well established that VEGFA/VEGFR2 is the primary signalling for angiogenesis, but its function typically requires the binding of VEGF-C and VEGFR2, while VEGFR3 functions as a trapper of VEGF-C, thus inhibiting VEGFR2 signalling (Hamada *et al.,* 2000). Therefore, TDF and other NRTI treatments may restrain VEGF-C-induced neovessel formation by enhancing the binding of VEGF-C to VEGFR3 in endothelial cells. On the other hand, the suppression by NRTIs of FGF-induced angiogenesis may be partly due to the blockage of the FGF signalling-maintained VEGFR2 expression (Murakami *et al.,* 2011) and an effect on the docking protein FRS2α that would adapt the crosstalk between the two RTK pathways (Chen *et al.,* 2014). Since the dose of NRTIs in the present study was similar to the serum concentration found in clinical treatments, these experimental phenotypes may reflect the development of endothelial dysfunction and impairments in angiogenesis/lymphangiogenesis in patients receiving ART therapy.

The present study demonstrated that NRTI treatment suppresses the activation of the pathways through systematic effects on protein maturation, receptor phosphorylation and their downstream signal transduction pathways respectively. Notably, NRTIs affect VEGFR2, VEGFR3 and FGFR1, which are categorized as RTKs. However, NRTIs have little effect on the signalling of other endothelial membrane receptors, such as the NOTCH pathway. Thus, NRTIs negatively regulate EC growth by selectively dampening vascular growth factor-mediated RTK signalling. To further investigate this regulatory mechanism, the effects of NRTIs on RTK subcellular trafficking were investigated. Typically, RTKs are synthesized in the endoplasmic reticulum and subsequently transported onto the cell membrane *via* the Golgi apparatus

Figure 4

NRTIs attenuate RTK internalization and endocytosis in HMVECs and HDLECs. After labelling cell surface VEGFR2, FGFR1 and VEGFR3 with the corresponding antibodies in HMVECs or HDLECs, the cells were stimulated with VEGF-A165 (50 ng·mL^{-1}), bFGF (50 ng·mL^{-1}) or VEGF-C (50-ng·mL^{-1}) for 20 min, followed by the removal of remaining cell surface receptors by acid washing. Fixed cells were run on a FACS scan cytometer. An increase in fluorescence intensity represents internalized VEGFR2, FGFR1 or VEGFR3 as indicated. (A–C) Representative histograms of VEGFR2 internalization in HMVECs with TDF and AZT treatments are shown in (A) and (B), respectively, and the corresponding quantitative analysis is shown in (C). (D–F) Representative histograms of FGFR1 internalization in HMVECs with TDF and AZT treatments are shown in (D) and (E), respectively, and the corresponding quantitative analysis is shown in (F). (G–I) Representative histograms of VEGFR3 internalization in HDLECs with TDF and AZT treatments are shown in (G) and (H), respectively, and corresponding quantitative analysis is shown in (I). Data represent the means ± SEM from five independent experiments. *$P < 0.05$ versus control; ns, not significant. (J–L) HMVECs or HDLECs treated with or without TDF were stimulated with VEGF-A165 (50 ng·mL^{-1}), bFGF (200 ng·mL^{-1}) or VEGF-C (100 ng·mL^{-1}) for the indicated times and subsequently incubated with anti-VEGFR2, anti-FGFR1 or anti-VEGFR3 antibodies (green) together with anti-EEA1 antibody (red). Nuclei were stained with DAPI. Representative images for VEGFR2/EEA1, FGFR1/EEA1 and VEGFR3/EEA1 co-localization visualized using immunofluorescence microscopy are shown in (J), (L) and (N), respectively, and the corresponding quantitative analyses are shown in (K), (M) and (O). Data represent the means ± SEM of five independent experiments. Scale bar represents 15 μm. *$P < 0.05$ versus control; ns, not significant.

(Simons, 2012). Constitutive internalization is part of the regular RTK cycling but is much slower than the return to the cell surface. Accordingly, RTK maintains abundant responsiveness to extracellular ligands (Eichmann and Simons, 2012; Simons, 2012; Zhang et al., 2013). However, augmented endocytosis of endothelial RTKs is required for angiogenic signal transduction upon growth factor stimuli in vascular ECs (Eichmann and Simons, 2012). The key events during this process are the clathrin-dependent internalization of ligand-occupied RTKs and their subsequent trafficking into EEA1-positive early endosomes, where

downstream effectors of growth signalling are activated (Lanahan et al., 2010). Meanwhile, ECs launch the resorting of RTK either for degradation or recycling back to cell membrane (Simons, 2012). The present study demonstrated that NRTIs selectively block the entry of activated receptors into early endosomes, thereby disrupting angiogenic signalling in ECs. In contrast, the accumulation of RTKs on the cell membrane was not affected significantly by TDF and 3TC. Interestingly, AZT may define an important interfering step of NRTIs on RTK trafficking across the cell membrane. We observed that AZT induced an unique inhibitory effect on the
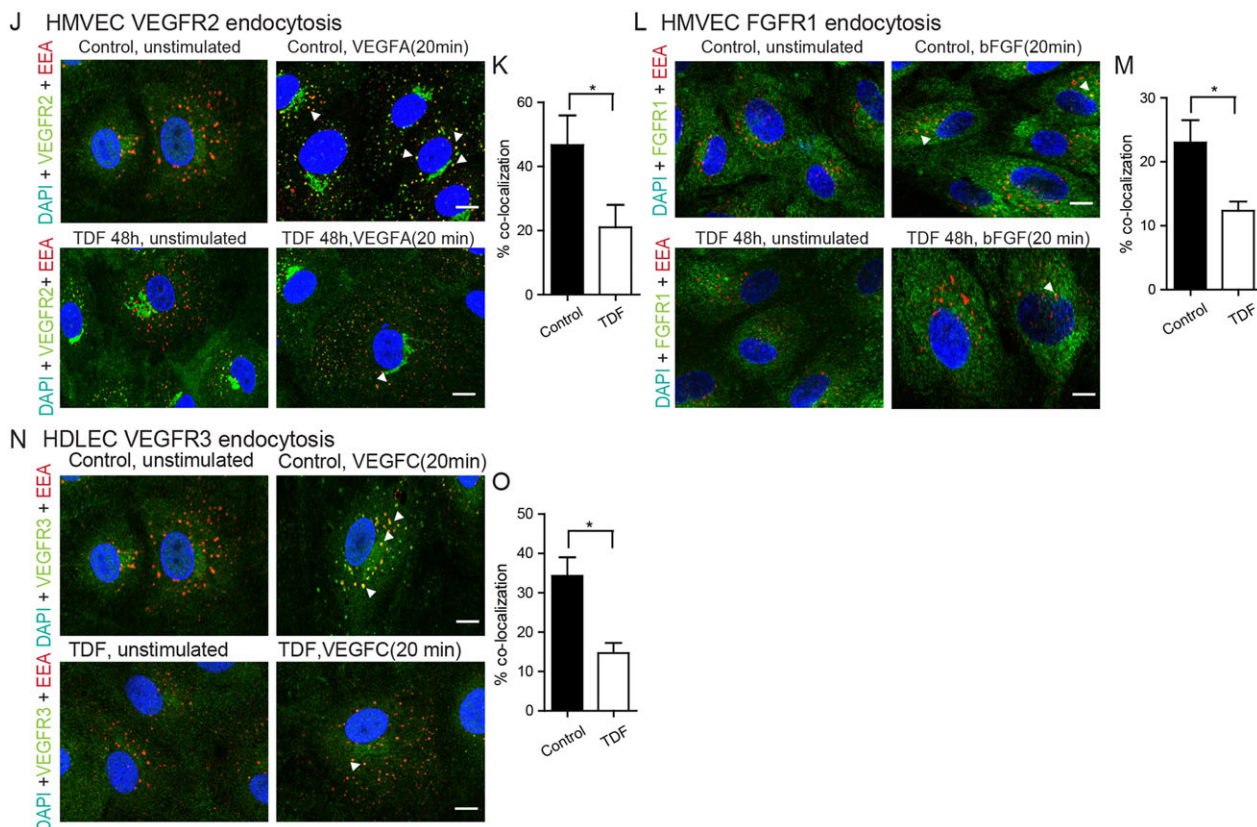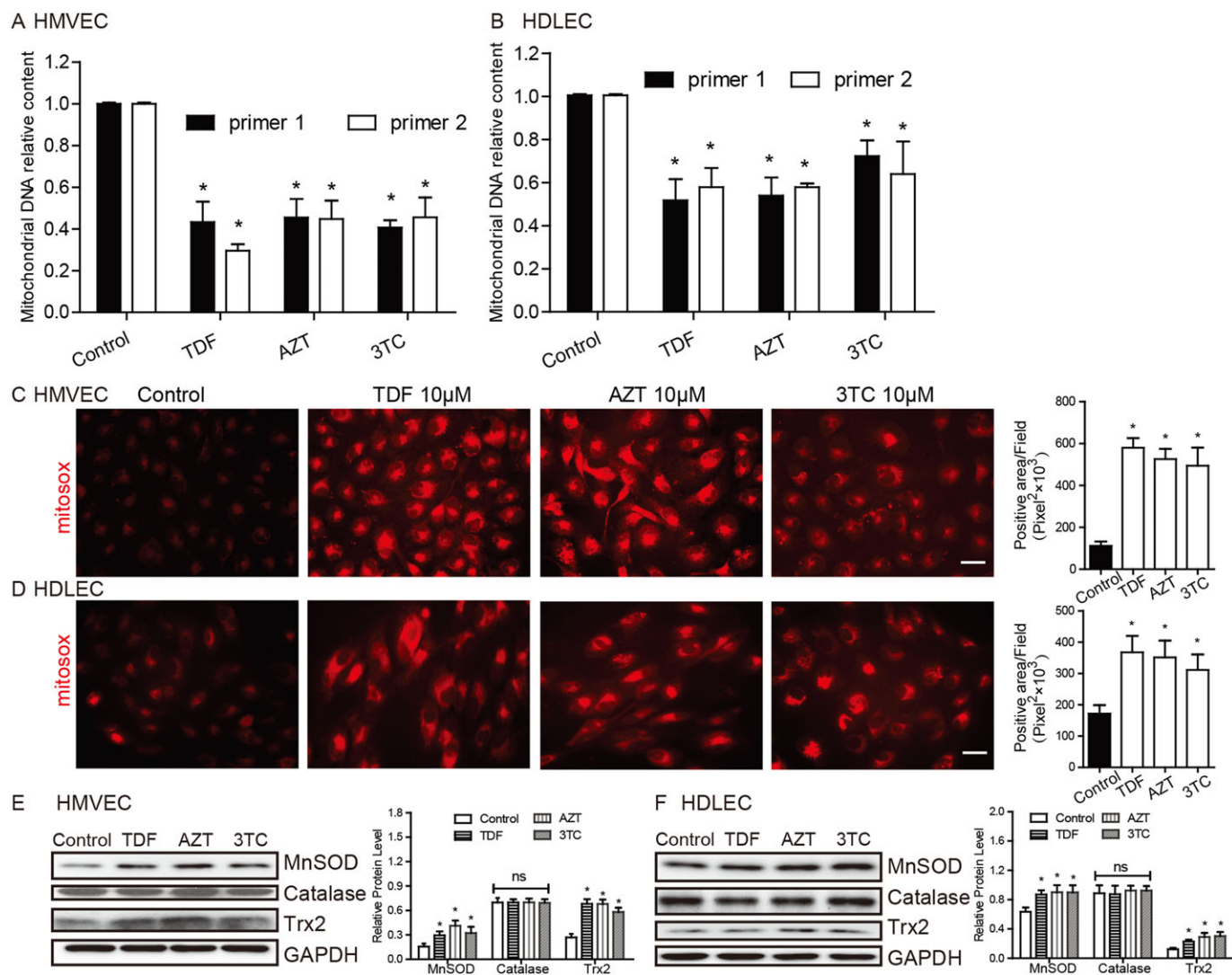
Figure 4

(Continued)

maturation of the RTKs, partially decreasing their glycosylation. Glycosylation of these receptors is essential for protein maturation and their retention on the cell membrane for phosphorylation/activation (Takahashi and Shibuya, 1997; Shen *et al.*, 1998; Markowska *et al.*, 2011). Therefore, AZT may disturb the surface expression and internalization of RTKs by evoking their deglycosylation. Details of this mechanism should be clarified in future studies.

Mitochondrial toxicity is a common side effect of ART (Chattopadhyay and Aldous, 2016; Selvaraj *et al.*, 2014). With regard to the adverse cellular effects of NRTIs, we hypothesized that the mitochondria provide modulatory signals, which contribute to the behaviour of ECs. Low-levels of ROS derived from cytosolic NADPH oxidases have been reported to play a physiological role in the regulation of normal endothelial signalling. The cytosolic ROS directly oxidizes tyrosine phosphatases and consequently promotes the sustained activation of RTK signalling involved in angiogenesis (Hamanaka and Chandel, 2010); therefore, ROS generation in response to physiological environmental cues may support the normal or compensatory function of endothelial cells (Sena and Chandel, 2012). In the present study, the MnSOD mimic MnTMPyP alleviated the NRTI-induced impairment of RTK signalling and angiogenic capability in ECs, suggesting that mitochondrial ROS may play a different role in angiogenesis. Compared with other cell types, the mitochondrial content in all ECs is low (2–6% of cytoplasm

volume). Indeed, endothelial mitochondria are considered to be signal centres rather than energy producers; mitochondrial ROS is a pivotal mediator of endothelial cell behaviour (Freed and Gutterman, 2013; Tang *et al.*, 2014). In the present and previous studies, NRTI treatment resulted in mitochondrial dysfunction and the excessive production of mitochondrial ROS. The pathological accumulation of mitoROS may thereby mediate mitochondrial fission/fusion (Suen *et al.*, 2008; Lugus *et al.*, 2011; Shen *et al.*, 2015), mitophagy (Tang *et al.*, 2014), amino acid (Dang, 2012; DeBerardinis and Thompson, 2012; Kalhan and Hanson, 2012; Phang and Liu, 2012; Shyh-Chang *et al.*, 2013) and fatty acid metabolization (Hulsmann and Dubelaar, 1988; Hulsmann and Dubelaar, 1992; Dagher *et al.*, 1999; Dagher *et al.*, 2001), all well-known mitochondria-related events involved in RTK signalling and angiogenesis. Moreover, NRTIs may induce the overproduction of mitoROS, which then initiates a vicious cycle that exacerbates mitochondrial dysfunction and induces the further release of mitoROS, resulting in KDR signalling defects in endothelial cells. Therefore, NRTI-induced excessive mROS may act as a specific pathological signal in EC growth and angiogenesis.

In the present study, we identified the adverse effects of NRTIs, the most common class of ART in HIV infection, on vascular growth and development. In addition to the endothelial injury in arteriosclerosis, as the major concern of ART treatment, recent studies have also demonstrated other

Figure 5

NRTIs induce oxidative stress due to dysfunctional mitochondria in HMVECs and HDLECs. After TDF, AZT or 3TC treatment for 48 h, mitochondrial DNA copy number was assessed in HMVECs (A) and HDLECs (B). Data represent the means ± SEM of five independent experiments. *$P < 0.05$ versus control. (C–D) After TDF, AZT or 3TC treatment for 48 h, NRTI-induced an increase in mitochondrial ROS production, as determined using the mitochondria-targeted fluorescence probe mitoSOX. Representative images of HMVECs and HDLECs and corresponding quantitative analyses are shown in (C) and (D) for five independent experiments respectively. Scale bar represents 25 μm. (E, F) Cell lysates of control and NRTI-treated HMVECs and HDLECs were blotted with antibodies against MnSOD, catalase or Trx2. Representative images are shown in (E) and (F). Data in (E) and (F) represent the means ± SEM of five independent experiments relative to GAPDH determined using densitometry. *$P < 0.05$ versus control. ns, not significant.

side effects of ART, such as endothelial cell senescence, renal endothelial dysfunction, endothelial activation and effects on endothelial progenitor cells (Zhan *et al.*, 2016; Zungsontiporn *et al.*, 2016; Echeverria *et al.*, 2017; Meneses *et al.*, 2017). However, few studies have referred to the effect of ART on angiogenic capability of endothelial cells. To our knowledge, the present study is the first to systemically investigate the effect of ART on angiogenic characteristics of endothelial cells and vascular angiogenesis/lymphangiogenesis. These findings may apply to other ART drugs, such as protease inhibitors (PI) and integrase inhibitors, and suggest additional clinical strategies for preventing cardiovascular disease in AIDS patients with ART treatment. Moreover,

the anti-angiogenesis effect of NRTIs can be explored to manipulate tumour angiogenesis, as indicated in the study of PI on KS (Sgadari *et al.*, 2002). The combination of NRTIs and PI could be developed as a novel 'cocktail' for the treatment of virus-related tumours.

Acknowledgements
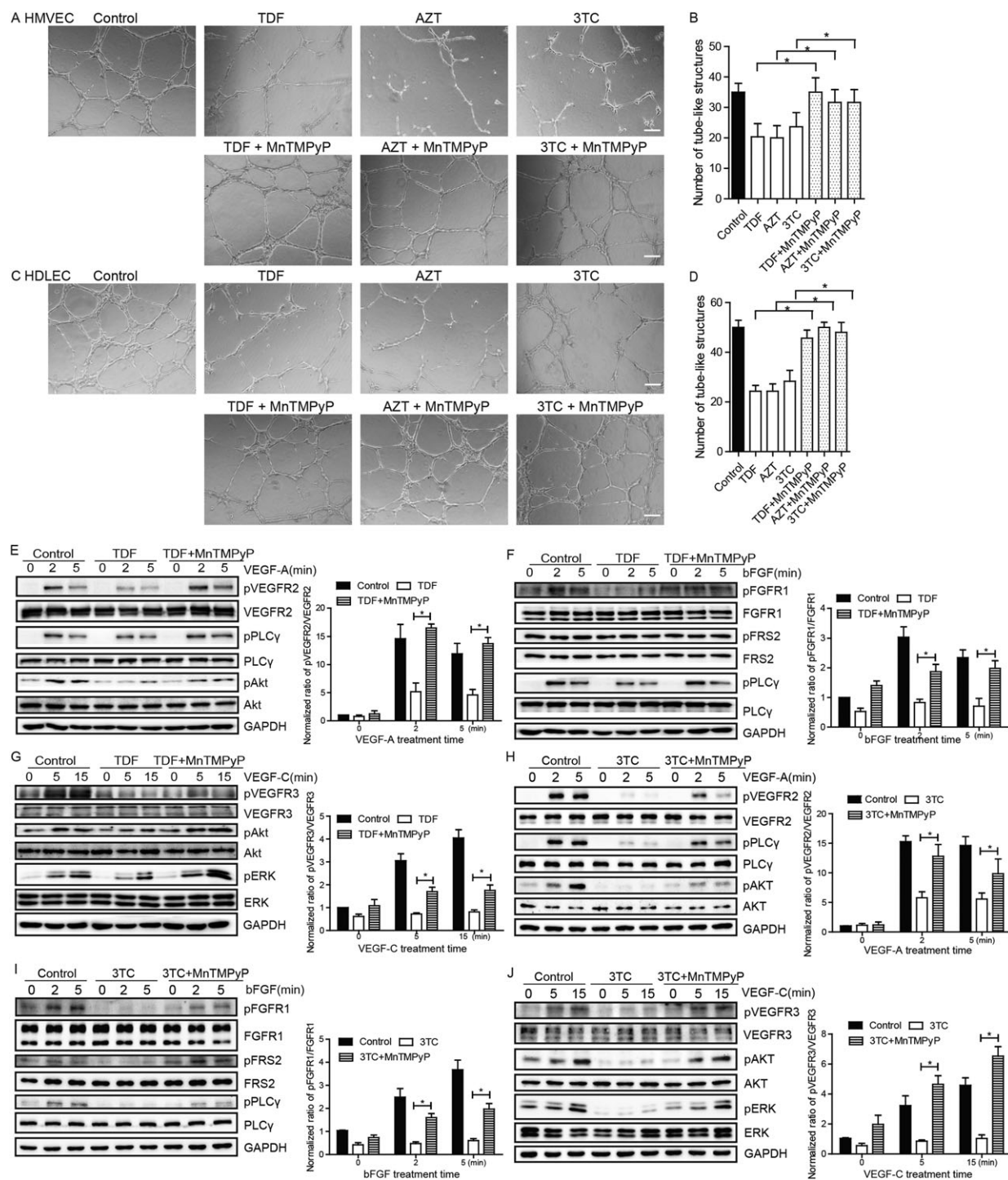
Figure 6

MnTMPyP alleviates NRTI-induced angiogenic and lymphangiogenic defects in HMVECs and HDLECs. (A–D) Effects of MnTMPyP on tube forma-tion in NRTI-treated HMVECs and HDLECs. HMVECs and HDLECs were treated with TDF, AZT or 3TC for 24 h and subsequently cultured without (control) or with MnTMPyP (2.5 μM) for 24 h. HMVECs or HDLECs were subsequently seeded in Matrigel for 6 h. Representative images are shown in (A) and (C). Branch points were quantified in (B) and (D). Data represent the means ± SEM from triplicates in each group from five independent experiments. Scale bar represents 100 μm. *$P < 0.05$. (E, F, H, I) Effects of MnTMPyP on VEGFR2 and FGFR1 signalling pathways in NRTI-treated HMVECs. HMVECs were treated with TDF or 3TC for 24 h and subsequently cultured without (control) or with MnTMPyP (2.5 μM) for 24 h. The activation of VEGFR2 and FGFR1 signalling pathways was determined as in Figure 3A, B. (G, J) Effects of MnTMPyP on VEGFR3 signalling pathway in NRTI-treated HDLECs. HDLECs were treated with TDF or 3TC for 24 h and subsequently cultured without (control) or with MnTMPyP (2.5 μM) for 24 h. The activation of VEGFR3 signalling pathway was determined as in Figure 3C. Representative images are shown in (E–J). Data in (E–J) represent mean ± SEM of five independent experiments relative to corresponding total proteins as determined by densitometry. *$P < 0.05$.

Author contributions

L.S., S.D., X.Z., C.Q., Y.W. and Y.S. performed the experiments and acquired the data. L.S., S.D., Z.G., X.Z. and C.Q. analysed the data and prepared the figures. L.S., S.D. and L.Y. drafted the sections of the paper. L.Y. conceived and designed the experiments. L.Y., Z.G., L.S. and S.D. prepared the final version of the manuscript. S.C. and W.Y. reviewed and proofread the manuscript. S.C., W.Y., Z.G., E.L. and Y.S. contributed the reagents/materials/analysis tools.

Conflict of interest

The authors declare no conflicts of interest.

Declaration of transparency and scientific rigour

This Declaration acknowledges that this paper adheres to the principles for transparent reporting and scientific rigour of preclinical research recommended by funding agencies, publishers and other organisations engaged with supporting research.

References

Adams RH, Alitalo K (2007). Molecular regulation of angiogenesis and lymphangiogenesis. Nature reviews. Mol Cell Biol 8: 464–478.

Alexander SPH, Kelly E, Marrion N, Peters JA, Benson HE, Faccenda E et al. (2015a). The Concise Guide to PHARMACOLOGY 2015/16: Overview. Br J Pharmacol 172: 5729–5743.

Alexander SPH, Fabbro D, Kelly E, Marrion N, Peters JA, Benson HE et al. (2015b). The Concise Guide to PHARMACOLOGY 2015/16: Catalytic receptors. Br J Pharmacol 172: 5979–6023.

Alexander SPH, Fabbro D, Kelly E, Marrion N, Peters JA, Benson HE et al. (2015c). The Concise Guide to PHARMACOLOGY 2015/16: Enzymes. Br J Pharmacol 172: 6024–6109.

Althoff KN, McGinnis KA, Wyatt CM, Freiberg MS, Gilbert C, Oursler KK et al. (2015). Comparison of risk and age at diagnosis of myocardial infarction, end-stage renal disease, and non-AIDS-defining cancer in HIV-infected versus uninfected adults. Clin Infect Dis: An Official Publication of the Infectious Diseases Society of America 60: 627–638.

Baker JV, Lundgren JD (2011). Cardiovascular implications from untreated human immunodeficiency virus infection. Eur Heart J 32: 945–951.

Beckstead JH, Wood GS, Fletcher V (1985). Evidence for the origin of Kaposi's sarcoma from lymphatic endothelium. Am J Pathol 119: 294–300.

Benedito R, Rocha SF, Woeste M, Zamykal M, Radtke F, Casanovas O et al. (2012). Notch-dependent VEGFR3 upregulation allows angiogenesis without VEGF-VEGFR2 signalling. Nature 484: 110–114.

Bhatti AB, Usman M, Kandi V (2016). Current scenario of HIV/AIDS, treatment options, and major challenges with compliance to antiretroviral therapy. Cureus 8: e515.

Bir SC, Kolluru GK, Fang K, Kevil CG (2012). Redox balance dynamically regulates vascular growth and remodeling. Semin Cell Dev Biol 23: 745–757.

Boccara F, Lang S, Meuleman C, Ederhy S, Mary-Krause M, Costagliola D et al. (2013). HIV and coronary heart disease: time for a better understanding. J Am Coll Cardiol 61: 511–523.

Chattopadhyay K, Aldous C (2016). A brief review on human mtDNA mutations and NRTI-associated mtDNA toxicity and mutations. Mitochondrial DNA. Part A, DNA mapping, sequencing, and analysis 27: 1685–1687.

Chen PY, Qin LF, Zhuang ZW, Tellides G, Lax I, Schlessinger J et al. (2014). The docking protein FRS2 alpha is a critical regulator of VEGF receptors signaling. P Natl Acad Sci USA 111: 5514–5519.

Chittick GE, Zong J, Blum MR, Sorbel JJ, Begley JA, Adda N et al. (2006). Pharmacokinetics of tenofovir disoproxil fumarate and ritonavir-boosted saquinavir mesylate administered alone or in combination at steady state. Antimicrob Agents Chemother 50: 1304–1310.

Choi I, Lee S, Hong YK (2012). The new era of the lymphatic system: no longer secondary to the blood vascular system. Cold Spring Harb Perspect Med 2: a006445.

Curtis MJ, Bond RA, Spina D, Ahluwalia A, Alexander SP, Giembycz MA et al. (2015). Experimental design and analysis and their reporting: new guidance for publication in BJP. Br J Pharmacol 172: 3461–3471.

Dagher Z, Ruderman N, Tornheim K, Ido Y (1999). The effect of AMP-activated protein kinase and its activator AICAR on the metabolism of human umbilical vein endothelial cells. Biochem Biophys Res Commun 265: 112–115.

Dagher Z, Ruderman N, Tornheim K, Ido Y (2001). Acute regulation of fatty acid oxidation and amp-activated protein kinase in human umbilical vein endothelial cells. Circ Res 88: 1276–1282.

Dang CV (2012). Links between metabolism and cancer. Genes Dev 26: 877–890.

DeBerardinis RJ, Thompson CB (2012). Cellular metabolism and disease: what do metabolic outliers teach us? Cell 148: 1132–1144.

Duchesne L, Tissot B, Rudd TR, Dell A, Fernig DG (2006). N-glycosylation of fibroblast growth factor receptor 1 regulates ligand and heparan sulfate co-receptor binding. J Biol Chem 281: 27178–27189.

Echeverria P, Gomez-Mora E, Roura S, Bonjoch A, Puig J, Perez-Alvarez N et al. (2017). Variable endothelial cell function restoration after initiation of two antiretroviral regimens in HIV-infected individuals. J Antimicrob Chemother 72: 2049–2054.

Eichmann A, Simons M (2012). VEGF signaling inside vascular endothelial cells and beyond. Curr Opin Cell Biol 24: 188–193.

Feige JJ, Baird A (1988). Glycosylation of the basic fibroblast growth factor receptor. The contribution of carbohydrate to receptor function. J Biol Chem 263: 14023–14029.

Freed JK, Gutterman DD (2013). Mitochondrial reactive oxygen species and vascular function: less is more. Arterioscler Thromb Vasc Biol 33: 673–675.

Freiberg MS, Chang CC, Kuller LH, Skanderson M, Lowy E, Kraemer KL et al. (2013). HIV infection and the risk of acute myocardial infarction. JAMA Intern Med 173: 614–622.

de Gaetano DK, Rabagliati R, Iacoviello L, Cauda R (2004). HIV infection, HAART, and endothelial adhesion molecules: current perspectives. Lancet Infect Dis 4: 213–222.

Gurzu S, Ciortea D, Munteanu T, Kezdi-Zaharia I, Jung I (2013). Mesenchymal-to-endothelial transition in Kaposi sarcoma: a histogenetic hypothesis based on a case series and literature review. PLoS One 8: e71530.

Hamada K, Oike Y, Takakura N, Ito Y, Jussila L, Dumont DJ et al. (2000). VEGF-C signaling pathways through VEGFR2 and VEGFR-3 in vasculoangiogenesis and hematopoiesis. Blood 96: 3793–3800.

Hamanaka RB, Chandel NS (2010). Mitochondrial reactive oxygen species regulate cellular signaling and dictate biological outcomes. Trends Biochem Sci 35: 505–513.

Hemkens LG, Bucher HC (2014). HIV infection and cardiovascular disease. Eur Heart J 35: 1373–1381.

Horowitz A, Simons M (2008). Branching morphogenesis. Circ Res 103: 784–795.

Hulsmann WC, Dubelaar ML (1988). Aspects of fatty acid metabolism in vascular endothelial cells. Biochimie 70: 681–686.

Hulsmann WC, Dubelaar ML (1992). Carnitine requirement of vascular endothelial and smooth muscle cells in imminent ischemia. Mol Cell Biochem 116: 125–129.

Jiang B, Hebert VY, Li Y, Mathis JM, Alexander JS, Dugas TR (2007). HIV antiretroviral drug combination induces endothelial mitochondrial dysfunction and reactive oxygen species production, but not apoptosis. Toxicol Appl Pharmacol 224: 60–71.

Jiang B, Hebert VY, Khandelwal AR, Stokes KY, Dugas TR (2009). HIV-1 antiretrovirals induce oxidant injury and increase intima-media thickness in an atherogenic mouse model. Toxicol Lett 187: 164–171.

Jiang B, Khandelwal AR, Rogers LK, Hebert VY, Kleinedler JJ, Zavecz JH et al. (2010). Antiretrovirals induce endothelial dysfunction via an oxidant-dependent pathway and promote neointimal hyperplasia. Toxicol Sci: An Official Journal of the Society of Toxicology 117: 524–536.

Kalhan SC, Hanson RW (2012). Resurgence of serine: an often neglected but indispensable amino Acid. J Biol Chem 287: 19786–19791.

Kilkenny C, Browne W, Cuthill IC, Emerson M, Altman DG (2010). Animal research: reporting in vivo experiments: the ARRIVE guidelines. Br J Pharmacol 160: 1577–1579.

Kim YW, Byzova TV (2014). Oxidative stress in angiogenesis and vascular disease. Blood 123: 625–631.

Koch S, Claesson-Welsh L (2012). Signal transduction by vascular endothelial growth factor receptors. Cold Spring Harb Perspect Med 2: a006502.

Lanahan AA, Hermans K, Claes F, Kerley-Hamilton JS, Zhuang ZW, Giordano FJ et al. (2010). VEGF receptor 2 endocytic trafficking regulates arterial morphogenesis. Dev Cell 18: 713–724.

Lang S, Mary-Krause M, Cotte L, Gilquin J, Partisani M, Simon A et al. (2010). Increased risk of myocardial infarction in HIV-infected patients in France, relative to the general population. AIDS 24: 1228–1230.

Lugus JJ, Ngoh GA, Bachschmid MM, Walsh K (2011). Mitofusins are required for angiogenic function and modulate different signaling pathways in cultured endothelial cells. J Mol Cell Cardiol 51: 885–893.

Marcelo KL, Goldie LC, Hirschi KK (2013). Regulation of endothelial cell differentiation and specification. Circ Res 112: 1272–1287.

Markowska AI, Jefferies KC, Panjwani N (2011). Galectin-3 protein modulates cell surface expression and activation of vascular endothelial growth factor receptor 2 in human endothelial cells. J Biol Chem 286: 29913–29921.

Massimo Andreoni SM, Puro V, De Carli G, Tambussi G, Nozza S, Gori A (2015). An update on integrase inhibitors: new opportunities for a personalized therapy? The NEXTaim Project. New Microbiol 38: 443–490.

McColl BK, Stacker SA, Achen MG (2004). Molecular regulation of the VEGF family – inducers of angiogenesis and lymphangiogenesis. APMIS: Acta Pathologica, Microbiologica, et Immunologica Scandinavica 112: 463–480.

McGrath JC, Lilley E (2015). Implementing guidelines on reporting research using animals (ARRIVE etc.): new requirements for publication in BJP. Br J Pharmacol 172: 3189–3193.

Meneses GC, Cavalcante MG, da Silva Junior GB, Martins AMC, Neto R, Liborio AB et al. (2017). Endothelial glycocalyx damage and renal dysfunction in HIV patients receiving combined antiretroviral therapy. AIDS Res Hum Retroviruses 33: 703–710.

Murakami M, Nguyen LT, Hatanaka K, Schachterle W, Chen PY, Zhuang ZW et al. (2011). FGF-dependent regulation of VEGF receptor 2 expression in mice. J Clin Invest 121: 2668–2678.

Phang JM, Liu W (2012). Proline metabolism and cancer. Front Biosci 17: 1835–1845.

Ray AS, Fordyce MW, Hitchcock MJ (2016). Tenofovir alafenamide: a novel prodrug of tenofovir for the treatment of human immunodeficiency virus. Antiviral Res 125: 63–70.

Reyskens KM, Essop MF (2014). HIV protease inhibitors and onset of cardiovascular diseases: a central role for oxidative stress and dysregulation of the ubiquitin-proteasome system. Biochim Biophys Acta 1842: 256–268.

Roy L, Sutliff SD, Weiss D, Parker J, Raidel S, Racine AK et al. (2002). Nucleoside reverse transcriptase inhibitors impair endothelium-dependent relaxation by increasing superoxide. Am J Physiol Heart Circ Physiol 283: H2363–H2370.

Selvaraj S, Ghebremichael M, Li M, Foli Y, Langs-Barlow A, Ogbuagu A et al. (2014). Antiretroviral therapy-induced mitochondrial toxicity: potential mechanisms beyond polymerase-gamma inhibition. Clin Pharmacol Ther 96: 110–120.

Sena LA, Chandel NS (2012). Physiological roles of mitochondrial reactive oxygen species. Mol Cell 48: 158–167.

Sgadari C, Barillari G, Toschi E, Carlei D, Bacigalupo I, Baccarini S et al. (2002). HIV protease inhibitors are potent anti-angiogenic molecules and promote regression of Kaposi sarcoma. Nature medicine 8: 225–232.

Shah MR, Cook N, Wong R, Hsue P, Ridker P, Currier J et al. (2015). Stimulating high impact HIV-related cardiovascular research:

recommendations from a multidisciplinary NHLBI Working Group on HIV-related heart, lung, and blood disease. J Am Coll Cardiol 65: 738–744.

Shen BQ, Lee DY, Gerber HP, Keyt BA, Ferrara N, Zioncheck TF (1998). Homologous up-regulation of KDR/Flk-1 receptor expression by vascular endothelial growth factor *in vitro*. J Biol Chem 273: 29979–29985.

Shen T, Wang N, Yu X, Shi J, Li Q, Zhang C *et al*. (2015). The critical role of dynamin-related protein 1 in hypoxia-induced pulmonary vascular angiogenesis. J Cell Biochem 116: 1993–2007.

Shyh-Chang N, Locasale JW, Lyssiotis CA, Zheng Y, Teo RY, Ratanasirintrawoot S *et al*. (2013). Influence of threonine metabolism on S-adenosylmethionine and histone methylation. Science 339: 222–226.

Simons M (2012). An inside view: VEGF receptor trafficking and signaling. Phys Ther 27: 213–222.

Simons M, Eichmann A (2015). Molecular controls of arterial morphogenesis. Circ Res 116: 1712–1724.

Southan C, Sharman JL, Benson HE, Faccenda E, Pawson AJ, Alexander SPH *et al*. (2016). The IUPHAR/BPS guide to PHARMACOLOGY in 2016: towards curated quantitative interactions between 1300 protein targets and 6000 ligands. Nucl Acids Res 44: D1054–D1068.

Suen DF, Norris KL, Youle RJ (2008). Mitochondrial dynamics and apoptosis. Genes Dev 22: 1577–1590.

Takahashi T, Shibuya M (1997). The 230 kDa mature form of KDR/Flk-1 (VEGF receptor-2) activates the PLC-g pathway and partially induces mitotic signals in NIH3T3 fibroblasts. Oncogene 14: 2079–2089.

Tang X, Luo YX, Chen HZ, Liu DP (2014). Mitochondria, endothelial cell function, and vascular diseases. Front Phys 5: 175.

Triant VA, Lee H, Hadigan C, Grinspoon SK (2007). Increased acute myocardial infarction rates and cardiovascular risk factors among patients with human immunodeficiency virus disease. J Clin Endocrinol Metab 92: 2506–2512.

Ushio-Fukai M, Nakamura Y (2008). Reactive oxygen species and angiogenesis: NADPH oxidase as target for cancer therapy. Cancer Lett 266: 37–52.

Wang Y, Nakayama M, Pitulescu ME, Schmidt TS, Bochenek ML, Sakakibara A *et al*. (2010a). Ephrin-B2 controls VEGF-induced angiogenesis and lymphangiogenesis. Nature 465: 483–486.

Wang Y, Oliver G (2010b). Current views on the function of the lymphatic vasculature in health and disease. Genes Dev 24: 2115–2126.

Xue SY, Hebert VY, Hayes DM, Robinson CN, Glover M, Dugas TR (2013). Nucleoside reverse transcriptase inhibitors induce a mitophagy-associated endothelial cytotoxicity that is reversed by coenzyme Q10 cotreatment. Toxicol Sci: An Official Journal of the Society of Toxicology 134: 323–334.

Yang C, Mwaikambo BR, Zhu T, Gagnon C, Lafleur J, Seshadri S *et al*. (2008). Lymphocytic microparticles inhibit angiogenesis by stimulating oxidative stress and negatively regulating VEGF-induced pathways. Am J Phys Regul Integr Comp Phys 294: R467–R476.

Zarkada G, Heinolainen K, Makinen T, Kubota Y, Alitalo K (2015). VEGFR3 does not sustain retinal angiogenesis without VEGFR2. Proc Natl Acad Sci U S A 112: 761–766.

Zhan JX, Qin SS, Lu LL, Hu XM, Zhou J, Sun YY *et al*. (2016). miR-34a is a common link in both HIV- and antiretroviral therapy-induced vascular aging. Aging-Us 8: 3298–3310.

Zhang X, Lanahan AA, Simons M (2013). VEGFR2 trafficking: speed doesn't kill. Cell Cycle 12: 2163–2164.

Zhou Y, Yan H, Guo M, Zhu J, Xiao Q, Zhang L (2013). Reactive oxygen species in vascular formation and development. Oxid Med Cell Longev 2013: 374963.

Zungsontiporn N, Tello RR, Zhang G, Mitchell BI, Budoff M, Kallianpur KJ *et al*. (2016). Non-classical monocytes and monocyte chemoattractant protein-1 (MCP-1) correlate with coronary artery calcium progression in chronically HIV-1 infected adults on stable antiretroviral therapy. PLoS One 11: e0149143.

Supporting Information

Additional Supporting Information may be found online in the supporting information tab for this article.

https://doi.org/10.1111/bph.14036

Figure S1 Effects of NRTI treatment on proliferation, migration and tube formation in HUVECs. (A) The combination of Annexin V/PI staining and flow cytometric analysis of separation of normal, necroptotic, early and late apoptotic cell populations after TDF, AZT and 3TC treatment for 48 h. (B-C) After TDF, AZT or 3TC treatment for 48 h, confluent monolayers of HUVECs were subjected to wound healing assay. Representative images are shown in B and % wound closure was quantified in C. Data represent the means ± SEM; Data represent the means ± SEM based on 5 independent experiments. Scale bar, 200 μm. *$P < 0.05$ *vs*. control. (D) After TDF, AZT or 3TC treatment for 48 h, cell proliferation of HUVECs was measured using the Cell Counting Kit-8 assay. Data represent the means ± SEM from triplicates in each group from 5 independent experiments. *$P < 0.05$ *vs*. control. (E-F) After TDF, AZT or 3TC treatment for 48 h, HUVECs were subjected to transwell migration assay. Eight hours later, cells on the reverse side of the membrane were stained with crystal violet. Representative images are shown in E. Migratory cells were quantified in F. Data represent the means ± SEM from duplicates (6 different areas in each well) from 5 independent experiments. Scale bar, 100 μm. *$P < 0.05$ *vs*. control. (G-H) Tube formation assay in a Matrigel. After TDF, AZT or 3TC treatment for 48 h, HUVECs were seeded onto Matrigel for six hours and representative images are shown in G. Branch points were quantified in H. Data represent the means ± SEM from triplicates in each group from 5 independent experiments. Scale bar, 100 μm. *$P < 0.05$ *vs*. control.

Figure S2 Microfilament organization was disrupted by NRTIs. Microfilaments of HMVECs, HUVECs and HDLECs were detected using Actin-Tracker Green. Representative images are shown in A-C, respectively. The data in A-C are based on 5 independent experiments. Scale bar, 25 μm.

Figure S3 Matrigel mixed with either PBS (control), VEGF-A164 (50 ng·mL⁻¹), bFGF (100 ng·mL⁻¹) or VEGF-C (100 ng·mL⁻¹) was placed subcutaneously in C57BL/6 mice previously fed with distilled water (control), AZT (100 mg·kg⁻¹) or 3TC (100 mg·kg⁻¹) for 5 days. On day 10, Matrigel plugs were harvested and recorded using stereomicroscopy. Representative images of plugs are shown in panels A, D, G, J, M and P, respectively. Matrigel plugs were subsequently sectioned,

vascular and lymphatic vessels were subsequently assessed using immunofluorescence staining with anti-CD31 and anti-LYVE-I, respectively. Representative images of plugs with Ad-VEGF-A164, Ad-bFGF, and Ad-VEGF-C are shown in panels B, E, H, K, N and Q, respectively. Positive areas of new microvessels was quantified in C, F, I, L, O and R. Data represent the means ± SEM; $n = 6$ mice per group. Scale bar represents 50 μm. *$P < 0.05$ *vs.* control.

Figure S4 NRTI treatment blocks RTK pathways in HUVECs. (A-C) Control and NRTI-treated HUVECs were serum-starved overnight and treated with VEGF-A165 (50 ng·mL^{-1}) as indicated. Cell lysates were blotted with p-VEGFR2, VEGFR2, p-PLCγ, PLCγ, p-Akt, Akt, p-ERK, ERK antibodies, respectively. (D-F) Control and NRTI-treated HUVECs were serum-starved overnight and treated with bFGF (100 ng·mL^{-1}) as indicated. Cell lysates were blotted with p-FGFR1, FGFR1, p-PLCγ, PLCγ, p-FRS2, FRS2, p-Akt, Akt, p-ERK, ERK antibodies, respectively. (G) Cell lysates of control and NRTI-treated HUVECs were blotted with Notch1 and Hes1 antibodies, respectively. Representative images in A-G were obtained from 5 independent experiments. Data in A-G represent the means ± SEM of 5 independent experiments relative to corresponding total proteins in A-F and relative to GAPDH in G as determined by densitometry. *$P < 0.05$ *vs.* control. ns, not significant. NRTI treatment blocks RTK pathways in Matrigel in mice. Matrigel mixed with PBS, VEGF-A165 (50 ng/ml), bFGF (100 ng/ml) or VEGF-C (100 ng/ml) were injected into the subcutaneous tissues of mice. (H) Lysates of Matrigel with PBS or VEGF-A165 were blotted with p-VEGFR2, VEGFR2, p-PLCγ, PLCγ antibodies. (I) Lysates of Matrigel with PBS or bFGF were blotted with p-FGFR1, FGFR1, p-FRS2, FRS2 antibodies. (J) Lysates of Matrigel with PBS or VEGF-C were blotted with p-VEGFR3, VEGFR3, p-ERK, ERK antibodies.

Figure S5 Effects of AZT treatment on VEGFR2 and FGFR1 glycosylation. HMVECs were treated with AZT or tunicamycin (TM), an antibiotic that specifically inhibits the N-glycosylation of proteins. Cell lysates were blotted with VEGFR2 and GAPDH antibodies (A) or FGFR1 and GAPDH antibodies (B).

Figure S6 NRTIs attenuate RTK internalization and endocytosis in HUVECs. After labelling cell surface VEGFR2 or FGFR1 with anti-VEGFR2 (PE conjugated) or anti-FGFR1 (followed with Alexa Fluor 488 secondary antibody), respectively, in HUVECs, the cells were stimulated with VEGF-A165 (50 ng·mL^{-1}) or bFGF (50 ng·mL^{-1}) for 20 min, followed by removal of remaining cell surface receptors by acid washing. Fixed cells were run on a FACS can cytometer. Increase in fluorescence intensity represents internalized VEGFR2 or FGFR1 as indicated. (A-C) Representative histograms of VEGFR2 internalization in HUVECs with TDF or AZT treatment are shown in A and B, respectively, and the corresponding quantitative analysis is shown in C. (D-F) Representative histograms of FGFR1 internalization in HUVECs with TDF or AZT treatment are shown in D and E, respectively, and the corresponding quantitative analysis is shown in F. Data represent the means ± SEM based on 5 independent experiments. *$P < 0.05$ *vs.* control. ns, not significant. (G-J) HUVECs treated with or without TDF were stimulated with VEGF-A165 (50 ng·mL^{-1}) or bFGF (200 ng·mL^{-1}) for the

indicated times and subsequently incubated with anti-VEGFR2 or anti-FGFR1 antibodies (green), respectively, together with anti-EEA1 antibody (red). Nuclei were stained with DAPI. Representative images for VEGFR2/EEA1 or FGFR1/EEA1 co-localization visualized by immunofluorescence microscopy are shown in G and I, respectively, and the corresponding quantitative analyses are shown in H or J. Data represent the means ± SEM of 5 independent experiments. Scale bar, 15 μm. *$P < 0.05$ *vs.* control. ns, not significant.

Figure S7 Effects of NRTI treatment on RTK surface expression. After labelling cell surface with VEGFR2, FGFR1 or VEGFR3 with corresponding antibodies in HMVECs or HDLECs, the cells were rinsed with ice-cold PBS (pH 7.4 or pH 2.5, respectively). Fixed cells were run on a FACS can cytometer. The surface expression of RTKs was determined by quantifying the difference between total and internalized amount. (A-B) Representative histograms of VEGFR2 surface expression in HMVECs with or without AZT treatment are shown in A and corresponding quantitative analysis is shown in B. (C-D) Representative histograms of FGFR1 surface expression in HMVECs with or without AZT treatment are shown in C and the corresponding quantitative analysis is shown in D. (E-F) Representative histograms of VEGFR3 internalization in HDLECs with or without AZT treatment are shown in E and corresponding quantitative analysis is shown in F.

Figure S8 NRTIs induce mitochondrial dysfunction in HUVECs. (A) After TDF, AZT or 3TC treatment for 48 h, mitochondrial DNA copy number was assessed in HUVECs. Data represent the means ± SEM based on 5 independent experiments. *$P < 0.05$ *vs.* control. (B) After TDF, AZT or 3TC treatment for 48 h, the NRTI-induced increase in mitochondrial ROS production was verified using the mitochondria-targeted fluorescence probe mitoSOX. Representative images of HUVECs and the corresponding quantitative analysis are shown in B. Scale bar, 25 μm. (C) Cell lysates of control and NRTI-treated HUVECs were blotted with MnSOD, Catalase, and Trx2 antibodies, respectively. Representative images are shown in C. Data in C represent the means ± SEM of 5 independent experiments relative to GAPDH as determined by densitometry. *$P < 0.05$ *vs.* control. ns, not significant.

Figure S9 MnTMPyP rescues NRTIs induced angiogenic defect in HUVECs. (A-B) Effects of MnTMPyP on tube formation in NRTI-treated HUVECs. HUVECs were treated with TDF, AZT or 3TC for 24 h and subsequently cultured without (control) or with MnTMPyP (2.5 μM) for 24 h. HUVECs were subsequently seeded onto Matrigel for 6 h. Representative images are shown in A. Branch points were quantified in B. Data represent the means ± SEM from triplicates in each group from 5 independent experiments. Scale bar, 100 μm. *$P < 0.05$. (C-D) Effects of MnTMPyP on VEGFR2 and FGFR1 signalling pathways in NRTI-treated HUVECs. HUVECs were treated with TDF for 24 h and subsequently cultured without (control) or with MnTMPyP (2.5 μM) for 24 h. The activation of VEGFR2 and FGFR1 signalling pathway were determined as in Figure 3(A) and 3(B). Representative images are shown in C and D. Data in C and D represent the means ± SEM of 5 independent experiments relative to corresponding total protein as determined by densitometry. *$P < 0.05$.